Biomagnetism

1 author:

Jaakko Malmivuo
Technische Universität Berlin
646 PUBLICATIONS **4,239** CITATIONS

Some of the authors of this publication are also working on these related projects:

Complete Archive of Ragnar Granit's Scientific Publications View project

Electrocardiology View project

Wiley Encyclopedia of Electrical and Electronics Engineering

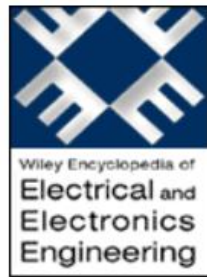## 24 Volume Set plus Supplement 1

John G. Webster

Wiley Encyclopedia of Electrical and Electronics Engineering

Book Title

Wiley Encyclopedia of Electrical and Electronics Engineering

SEARCH

All content

Advanced >   Saved Searches >
Search in this Book >

ARTICLE TOOLS

Save to My Profile

Export Citation for this Article

E-mail Link to this Article

Share

| Abstract | Article | Figures | References | Other Versions |

View Full Article (HTML) | Get PDF (4277K)

Abstract

Biomagnetic fields are generated by the same phenomenon as the bioelectric fields. They are induced by the electric currents generated by the activating tissues. These are primarily nerve and muscle tissues. The theoretical difference between these fields is based on the distribution of the elements of the volume sources generating these fields. Bioelectric and biomagnetic fields are generated by the flux and vortex source distributions, respectively. Although the flux and vortex source distributions are independent, the fields they generate are only partially independent. This means that with the biomagnetic measurement it is possible to obtain only partially new independent information on the source in addition to the bioelectric measurement. This is the fundamental issue in the application of biomagnetic methods and this will be discussed in detail in this article. In addition to the theoretical difference, bioelectric and biomagnetic methods have technical differences due to the different technologies that they use. This issue is also discussed in this article.

Keywords:
biomagnetism; bioelectricity; independent information

View Full Article (HTML) | Get PDF (4277K)

More content like this

Topics: Biomedical Engineering

BIOMAGNETISM

1. INTRODUCTION

Biomagnetism discusses the following electromagnetic and magnetic phenomena, which arise in biological tissues:

- The magnetic field at and beyond the body
- The response of excitable cells to magnetic field stimulation
- The intrinsic magnetic properties of the tissue

The magnetic field may be generated by both the bioelectric currents and magnetic material in the body. Similarly, by feeding magnetic energy to the body, it induces electric currents that may stimulate electrically excitable cells and magnetizes magnetic material in the body (provided that it has high enough intensity). In biomagnetic measurements they are the bioelectric currents, and in magnetic stimulation they are the induced stimulating electric currents in the body that are the main subjects of interest in biomagnetism. The magnetic fields due to magnetic material are not discussed in this article.

The biomagnetic and bioelectric fields are, of course, connected through Maxwell's equations. Therefore, the discussion on biomagnetism cannot be made without also discussing bioelectricity. When discussing the properties of the bioelectric and biomagnetic fields, two *theoretical issues* will have major role:

- First, *to get new information* from the bioelectric sources with a magnetic method the measurement sensitivity distribution of the magnetic measurement must be different from that of an electric measurement.
- Second, *to get with the magnetic measurement more accurate information* of the source distribution it must have better ability to concentrate its measurement sensitivity to a smaller region than the electric method.

It is not self-evident that the two aforementioned requirements are met with a biomagnetic measurement system.

There are also other issues in addition to the aforementioned *theoretical issues*, which may justify the use of biomagnetic methods. These are the *technical issues*. They are consequences from the different technology used in the detection of magnetic fields:

- First, the magnetic field detector may not contact the body surface.
- Second, because superconducting technology is used, the magnetic detector is capable of measuring DC fields (fields down to 0 Hz).

The main application areas of biomagnetic measurements are the measurements of the magnetic field generated by the heart, the magnetocardiogram (MCG), and the magnetic field generated by the brain, the magnetoencephalogram (MEG). The fundamental issue in the clinical application of biomagnetism is how much new information it brings in addition to that, which is obtained with bioelectric measurements. In other words, how independent the biomagnetic fields are from the bioelectric ones.

It will be shown on dipolar level that the diagnostic performance of biomagnetic and bioelectric measurements is similar. Furthermore, the three plus three elementary dipolar electric and magnetic leads are, on average, equal in diagnostic performance. When including them into the diagnostic system, it is on average the same in which order they are taken. The amount of additional information due to each additional lead decreases when the number of leads in the diagnostic system increases.

Due to reciprocity, the distribution of stimulation current density in magnetic stimulation is calculated with the same equations as the distribution of the measurement sensitivity. The great benefit of magnetic stimulation is that unlike in electric stimulation, the skull is "transparent" to the magnetic field and therefore the stimulation current density in the scalp region is of the same order as in the cortical region of the brain. Thus, the current density in the scalp is so low that it does not cause any sensation to the patient.

2. HISTORY

In 1819 professor Hans Christian Ørsted at the University of Copenhagen demonstrated to his students the heating of a platinum wire with electric current from a voltaic pile. During this demonstration he noticed that a nearby magnetized compass needle did move each time when the electric current was turned on. This was the first demonstration of the connection between electric current and magnetic field (1). In 1865 Scottish physicist James Clerk Maxwell derived the equations describing the connection between electric and magnetic fields (2).

Always, when there is an electric current, it induces a magnetic field. Similarly, the bioelectric currents always induce biomagnetic fields. Thus, the origin of biomagnetic fields is the same as the origin of bioelectric currents: the bioelectric activity of the tissue. However, the biomagnetic fields rise from different distribution of the bioelectric source elements than the bioelectric fields. Therefore, the biomagnetic signals include partially different information from the bioelectric volume source than the bioelectric signals (3).

Stimulation with electric current was made already in 1664 by Jan Swammerdam (4). This was over 100 years earlier than the popularly known experiments of Luigi Galvani (5).

The first detection of a bioelectric current was made by Carlo Matteucci by detecting the muscle impulse in 1838 (6) with the astatic galvanometer developed by Leopold Nobili in 1825 (7). The first detection of a biomagnetic field was made by Gerhard Baule and Richard McFee in 1963

(8). Magnetic stimulation was made for the first time in 1893 by Jacques d'Arsonval (9).

3. BIOELECTROMAGNETIC BACKGROUND

3.1. Source of Bioelectric Currents

Let us introduce the concept of the *impressed current density* $\boldsymbol{J}^{\mathrm{i}}$ (*x*, *y*, *z*, *t*). This is a nonconservative current that arises from the bioelectric activity of nerve and muscle cells due to the conversion of energy from chemical to electric form. The individual elements of this bioelectric source behave as electric current dipoles. Hence, the impressed current density equals the *volume dipole moment density* of the source. Note that $\boldsymbol{J}^{\mathrm{i}}$ is zero everywhere outside the region of active cells (10).

If the volume conductor is infinite and homogeneous and the conductivity is σ, the primary sources $\boldsymbol{J}^{\mathrm{i}}$ establish an electric field $\boldsymbol{E}$ and a conduction current $\sigma\boldsymbol{E}$. As a result, the total current density $\boldsymbol{J}$ (11) is given by equation 1:

$$\boldsymbol{J} = \boldsymbol{J}^{\mathrm{i}} + \sigma\boldsymbol{E} \qquad (1)$$

The quantity $\sigma\boldsymbol{E}$ is often referred to as the *return current*. This current is necessary to avoid buildup of charges due to the source current. Furthermore, the electric field $\boldsymbol{E}$ is *quasistatic*. That is, all currents and fields behave, at any instant, as if they were stationary. The description of the fields resulting from applied current sources is based on the understanding that the medium is resistive only, and that the phase of the time variation can be ignored (i.e., *all fields vary synchronously*).

Because the electric field $\boldsymbol{E}$ is quasistatic, it can be expressed at each instant of time as the negative gradient of a scalar potential Φ, and equation 1 may be rewritten as

$$\boldsymbol{J} = \boldsymbol{J}^{\mathrm{i}} - \sigma\nabla\Phi \qquad (2)$$

Since the tissue capacitance is negligible (quasistatic conditions), charges redistribute themselves in a negligibly short time in response to any source change. Since the divergence of $\boldsymbol{J}$ evaluates the rate of change of the charge density with respect to time, and since the charge density must be zero, the divergence of $\boldsymbol{J}$ is necessarily zero. (We refer to the total current $\boldsymbol{J}$ as being solenoidal or forming closed lines of current flow.) Therefore, equation 1 reduces to Poisson's equation:

$$\nabla \cdot \boldsymbol{J}^{\mathrm{i}} = \nabla \cdot \sigma\nabla\Phi + \nabla \cdot \boldsymbol{J} = \sigma\nabla^2\Phi \qquad (3)$$

The solution of equation 3 for the scalar function $\sigma\Phi$ for a region that is uniform and infinite in extent is (12):

$$4\pi\sigma\Phi = -\int_v (1/r)\nabla \cdot \boldsymbol{J}^{\mathrm{i}}\mathrm{d}v \qquad (4)$$

Because a source element $-\nabla \cdot \boldsymbol{J}^{\mathrm{i}}\mathrm{d}v$ in equation 4 behaves like a *point source*, in that it sets up a field, that varies as $1/r$, the expression $-\nabla \cdot \boldsymbol{J}^{\mathrm{i}}$ is defined as a

flow source density I_{F}. Because we seek the solution for field points outside the region occupied by the volume source, equation 4 may be transformed to (12):

$$4\pi\sigma\Phi = -\int_v \boldsymbol{J}^{\mathrm{i}} \cdot \nabla(1/r)\mathrm{d}v \qquad (5)$$

This equation represents the distribution of potential Φ due to the bioelectric source $\boldsymbol{J}^{\mathrm{i}}$ within an infinite, homogeneous volume conductor having conductivity σ. Here $\boldsymbol{J}^{\mathrm{i}}\mathrm{d}v$ behaves like a *dipole element* (with a field that varies as its dot product with $\nabla(1/r)$, and hence $\boldsymbol{J}^{\mathrm{i}}$ can be interpreted as a *volume dipole density*).

By using Green's theorem (13), David Geselowitz (11) developed equation 6, which evaluates the *electric potential* anywhere within an inhomogeneous volume conductor containing internal volume sources. The inhomogeneous volume conductor is modeled with a piecewise homogeneous volume conductor where the homogeneous regions are bounded by surfaces S_j. The values of conductivity σ with primed and double-primed symbols represent the conductivities for the inside and outside of each boundary, respectively.

$$4\pi\sigma\Phi(r) = \int_v \boldsymbol{J}^{\mathrm{i}} \cdot \nabla(1/r)\mathrm{d}v + \sum_j \int_{S_j} (\sigma''_j - \sigma'_j)\Phi\nabla(1/r) \cdot \mathrm{d}S_j$$

$$(6)$$

It is important to notice that the first term on the right-hand side of equation 6, involving $\boldsymbol{J}^{\mathrm{i}}$, represents the contribution of the volume source, and the second term represents the effect of the boundaries and inhomogeneities. The impressed source $\boldsymbol{J}^{\mathrm{i}}$ arises from cellular activity and hence has diagnostic value, whereas the second term can be considered a distortion due to the inhomogeneities of the volume conductor.

3.2. Biomagnetic Field

The current density $\boldsymbol{J}$ throughout a volume conductor gives rise to a magnetic field given by the following relationship (12, 14):

$$4\pi\boldsymbol{H} = \int_v \boldsymbol{J} \times \nabla(1/r)\mathrm{d}v \qquad (7)$$

where r is the distance from an external field point at which $\boldsymbol{H}$ is evaluated to an element of volume $\mathrm{d}v$ inside the body, $\boldsymbol{J}\mathrm{d}v$ is a source element, and ∇ is a vector differential operator with respect to the source coordinates. Substituting equation 2 into equation 7 and dividing the inhomogeneous volume conductor into homogeneous regions with surfaces S_j, we obtain

$$4\pi\boldsymbol{H} = \int_v \boldsymbol{J}^{\mathrm{i}} \times \nabla(1/r)\mathrm{d}v - \sum_j \int_{v_j} \sigma_j\nabla\Phi \times \nabla(1/r)\mathrm{d}v \qquad (8)$$

Again using Green's theorem and making some vector manipulations, we obtain equation 9

$$4\pi \boldsymbol{H}(r) = \int_v \boldsymbol{J}^i \times \nabla(1/r)\mathrm{d}v + \sum_j \int_{S_j} (\sigma_j'' - \sigma_j')\Phi\nabla(1/r) \times \mathrm{d}S_j$$

$$(9)$$

This equation describes the magnetic field outside a finite volume conductor containing internal (electric) volume sources $\boldsymbol{J}^i$ and inhomogeneities $(\sigma_j'' - \sigma')$. It was first derived by David Geselowitz (15).

Similarly as in equation 6 the first term on the right-hand side of equation 9, involving $\boldsymbol{J}^i$, represents the contribution of the volume source, and the second term the effect of the boundaries and inhomogeneities. The impressed source $\boldsymbol{J}^i$ arises from cellular activity and hence has diagnostic value, whereas the second term can be considered a distortion due to the inhomogeneities of the volume conductor.

Please note also that equations 6 and 9 describing the electric and magnetic fields due to the impressed current source distribution $\boldsymbol{J}^i$ are otherwise identical except that there exist the dot and cross-products, respectively.

Similarly, as discussed in connection with equation 6, it is easy to recognize that if the volume conductor is homogeneous, the difference $(\sigma_j'' - \sigma')$ in the second term in equation 9 is zero, and it drops out. Then the equations 6 and 9 reduce to the equations 5 and 7, the electric and magnetic fields in the case of *homogeneous* volume conductors, respectively.

3.3. Nature of Biomagnetic Sources

Equation 9 shows that the physiological phenomenon that is the source of the biomagnetic field is the *electric* activity of the tissue $\boldsymbol{J}^i$. Thus, for instance, the sources for the MCG or MEG are the *electric* activities of the cardiac muscle or nerve cells, respectively, as they are also the sources of the electrocardiogram (ECG) and electroencephalogram (EEG), respectively.

The difference between bioelectric and biomagnetic signals is seen from the form of their mathematical equations. When comparing equations 6 and 9, one can note that the electric field arises from the *divergence* and the magnetic field from the *curl* of the source. This distinction holds for both the first terms on the right-hand side of these equations arising from the distribution of impressed current and the second terms arising from the boundaries of the inhomogeneities of the volume source.

The theoretical difference between biomagnetic and bioelectric signals may also be seen from the difference in the *sensitivity distributions* of these measurements. The sensitivity distributions (the form of the lead fields) of magnetic and electric measurements are discussed in detail later.

It is pointed out that in the design of magnetic leads one must keep in mind the electric origin of the magnetic signal and the characteristic form of the sensitivity distribution of the magnetic measurement. If the lead of a magnetic measurement is not carefully designed, it is possible that its sensitivity distribution is similar to that of another electric lead. In such a case the magnetic measurement does not provide any new information about the source in addition to the electric measurement.

Note that the biomagnetic signals of the heart and the brain are assumed not to arise from magnetic material because such material does not exist in these tissues. There are special circumstances, however, where magnetic materials produce biomagnetic fields – for example, in the case of the signal due to the magnetic material contaminating the lungs of welders or the iron accumulating in the liver in certain diseases. Such fields are not discussed in this article.

4. LEAD FIELD THEORY

4.1. The Concept of Lead Field

The bioelectromagnetic differences between EEG and MEG may be explained by the different sensitivity distributions of electric and magnetic measurement methods (16). In an electric lead the lead field is an electric current field in the volume conductor generated by feeding a unit current to the lead. In a magnetic lead the current induced in a conductor depends on the rate of change of the magnetic flux that links the current loop. In analogy to the electric field case, the reciprocally energizing (time-varying) current I_r is normalized, so that its time derivative is unity for all values of ω. According to the reciprocity theorem of Helmholtz (17), *the current field produced in this manner in the volume conductor is identical to the distribution of the sensitivity of the lead*.

4.2. Capability of a Lead to Concentrate Its Measurement Sensitivity

Let us consider certain electric and magnetic leads whose geometric form is similar. If one of these has its measurement sensitivity concentrated in a smaller region, that is, is capable of measuring a source region with smaller dimensions or of localizing an equivalent dipole with better accuracy, it would be considered superior especially in brain research.

The comparison of the spatial resolutions of electric and magnetic recordings is made with the concept of *half-sensitivity volume*, HSV (16). This concept means the region in the source area where the detector sensitivity is one-half or more from the maximum sensitivity (in the source area). The smaller the HSV, the better is the detector's ability to focus its sensitivity to a small region. Such leads will be preferred especially in brain research.

5. INSTRUMENTATION

Biomagnetic fields have very low amplitude compared with the ambient noise fields and with the sensitivity of the detectors. A summary of these fields is shown in Figure 1 (18). The figure indicates that it is possible to detect the MCG with induction coil magnetometers, albeit with a
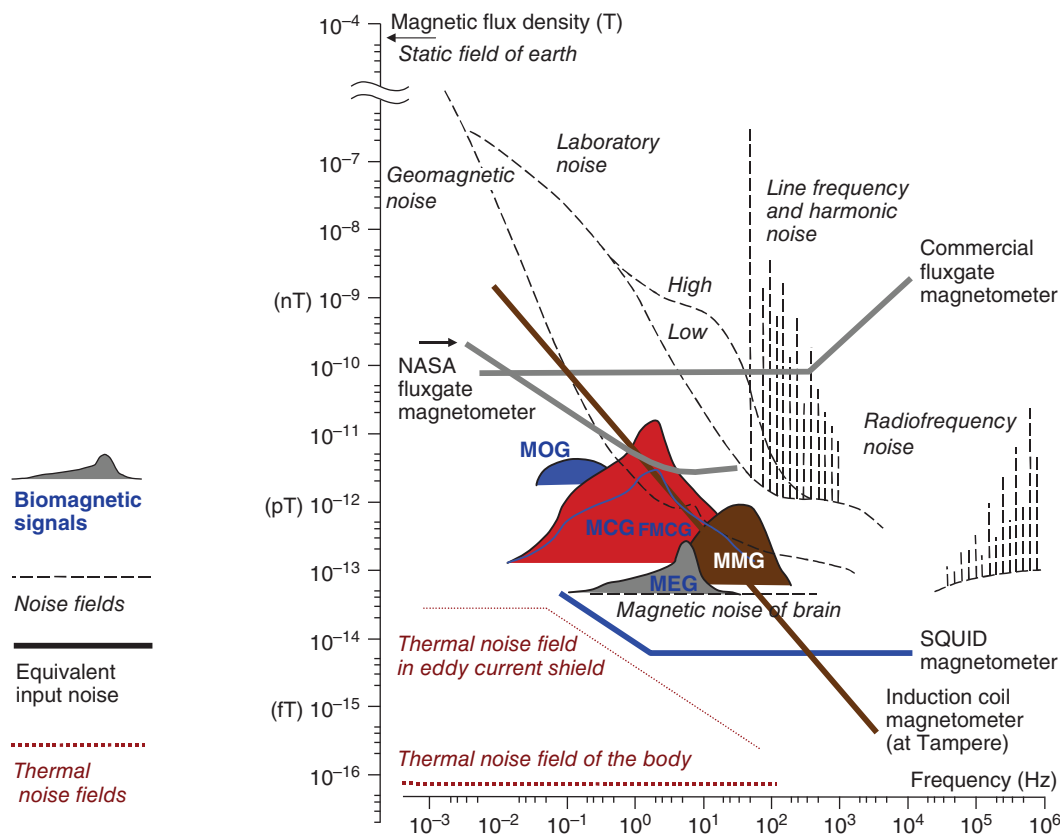
Figure 1. Magnetic signals produced by various sources. *Biomagnetic signals*: MCG = magnetocardiogram, MMG = magnetomyogram, MEG = magnetoencephalogram, MOG = magneto-oculogram. *Noise fields*: Static field of the Earth, Geomagnetic fluctuations, Laboratory noise, Line frequency noise, Radio frequency noise. *Equivalent input noise*: Commercial flux-gate magnetometer, Ring-core flux-gate (NASA), Induction coil magnetometer, SQUID-magnetometer. *Thermal noise fields*: Eddy current shield, The human body.

reasonably poor signal-to-noise ratio. However, even the most sensitive room temperature induction coil magneto-meter built for biomagnetic purposes (19) is not sensitive enough to detect the MEG for clinical use. Therefore, the Superconducting QUantum Interference Device (SQUID) is the only instrument that is sensitive enough for high-quality biomagnetic measurements. The instrumentation for measuring biomagnetic fields is not discussed further in this article. An overview of the modern instrumentation is published by Robbes (20).

6. MAGNETOCARDIOGRAPHY

6.1. Bioelectromagnetic Properties

Modeling the Cardiac Volume Source. In ECG and MCG it is the clinical problem to solve the inverse problem, that is, to solve the source of the detected signal in order to get information about the anatomy and physiology of the source. The clinical diagnostic procedure is actually based on measuring certain parameters, such as time intervals and amplitudes, from the detected signal and not on dis-playing the components of the source, like the x-, y-, and z-components of the vector cardiogram. Despite this, the selection of the source model is very important from the point of view of available information.

In clinical ECG, the source model is a dipole. This is the model for both the 12-lead ECG and vectorcardiography (VCG). The electric dipole moment of the volume source, that is, vector (electro)cardiogram, is detected with a detec-tor, whose lead field is composed of three orthogonal com-ponents, each being homogeneous and linear in the directions of the coordinate axes (Figure 2) (16). These are independent of each other, that is, it is not possible to synthesize one of them as a linear combination of the two other ones. Localization of a source is not possible with a lead whose sensitivity is homogeneously distributed. Such a lead can be used only for determining the magnitude and orientation of the dipolar electric source.

In 12-lead ECG, the volume conductor (thorax) model is not considered, which causes considerable distortion to the leads. In Frank VCG only the form of the volume conductor is modeled. This decreases the distortion in the lead fields but does not eliminate it completely. Note that today the display systems used in these ECG and vector electrocardiogram (VECG) systems do not play any role in the diagnostic procedure because the comput-erized diagnosis is always based on the signals, not on the display.

In selection of the source model for MCG, it is logical, at least initially, to select the magnetic source model to be dipole so that it is on the same theoretical level with the ECG.
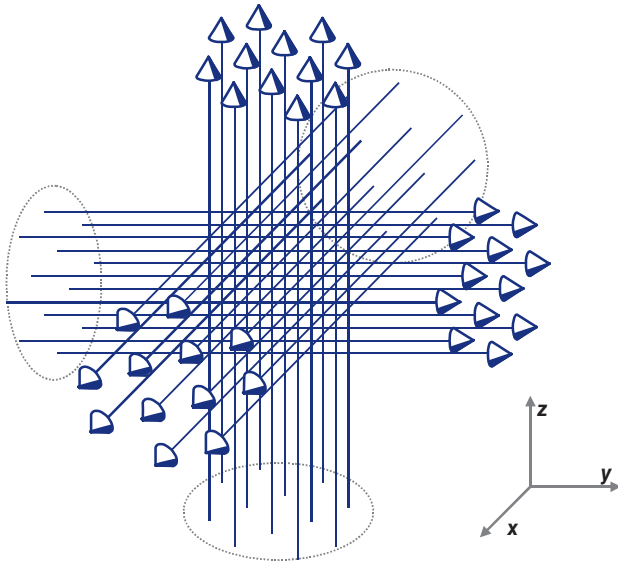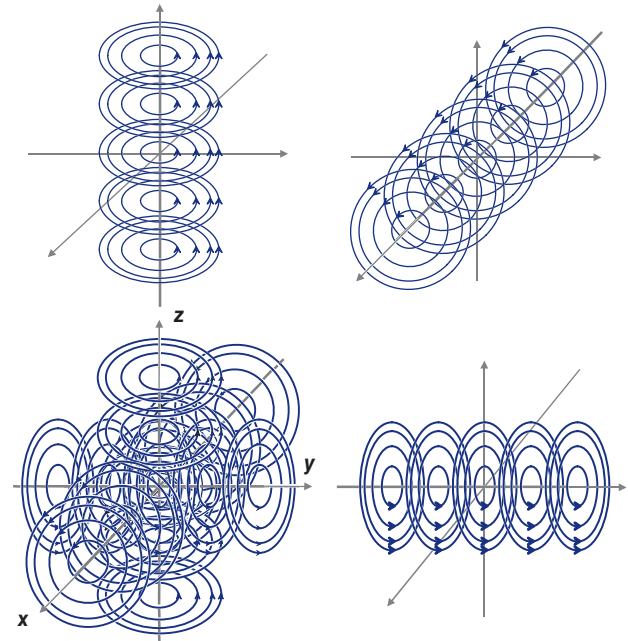
Figure 2. The lead field of a detector, which detects the electric dipole moment of a bioelectric volume source. It has three orthogonal components, each being homogeneous and linear in the directions of the coordinate axes.


Figure 3. The lead field of a detector, which detects the magnetic dipole moment of a bioelectric volume source. It has three orthogonal components, each having direction around the coordinate axes (symmetry axes) with the lead field current density (sensitivity) linearly proportional to the distance from the coordinate axis.

The magnetic dipole moment of the volume source, that is, vector magnetocardiogram, is detected with a detector, whose lead field is also composed of three orthogonal components, each being in tangential direction around the corresponding coordinate axis. The magnitude of the sensitivity is proportional to the radial distance from the symmetry axis. This sensitivity distribution is cylindrically symmetric so that when moving in the direction of the coordinate axis, it is unchanged (Figure 3) (16). Also, these are independent of each other, that is, it is not possible to synthesize one of them as a linear combination of the two other ones. Only in this way is it possible to compare the diagnostic performance of these methods. It is clear, of course, that if the source model is more accurate, that is, has more independent variables, the diagnostic performance is better, but when comparing ECG and MCG, the comparison is relevant only if their complexity, that is, number of independent variables, is similar (16).

Detection of the Equivalent Magnetic Dipole of the Heart. The basic detection method of the equivalent magnetic dipole moment of a volume source is to measure the magnetic field on each coordinate axis in the direction of that axis (Figure 4a). This is called the *XYZ*-lead system (21). To idealize the sensitivity distribution throughout the volume source, the measurements must be made at a distance that is large compared with the source dimensions. This, of course, decreases the signal amplitude. Much better way to increase the quality of the measurement is to use bipolar measurements, that is, measurements are made on both sides of the source (Figure 4b). Measurement of the magnetic field on all coordinate axes is, however, difficult to perform in MCG due to the geometry of the human body. Furthermore, it would require either

six sequential measurements with one magnetometer (dewar) or six simultaneous measurements using six dewars.

It has been shown (16, 21, 22) that all three components of the magnetic dipole can be measured from a single location (Figure 5a). This is called the *unipositional* method. It follows from the basic equations of the magnetic field that the *y*- and *z*-components have to be measured in the negative directions, and their magnitude has to be multiplied with factor 2 for all the three orthogonal components of the magnetic dipole to be measured with correct polarity and sensitivity. Applying this *unipositional* method symmetrically so that the measurements are made on both the anterior and posterior sides of the thorax at the same distance from the heart, only two dewars are needed and a very high quality of lead fields is obtained (Figure 5b). The dimensions and lead fields for the nonsymmetric and symmetric unipositional lead systems are shown in Figure 5c and d, respectively. Please note that the nonsymmetric unipositional lead system is sensitive mainly on the anterior side of the heart, whereas the symmetric unipositional lead system has almost perfect lead field.

Mapping the Cardiac Magnetic Field. In this article, it has been discussed the detection of the equivalent magnetic dipole of the cardiac volume source, the vector magnetocardiogram (VMCG). It has also been compared the diagnostic performance of this method with the detection of the equivalent electric dipole moment of the cardiac volume source, the VECG. Note that the diagnostic performance of
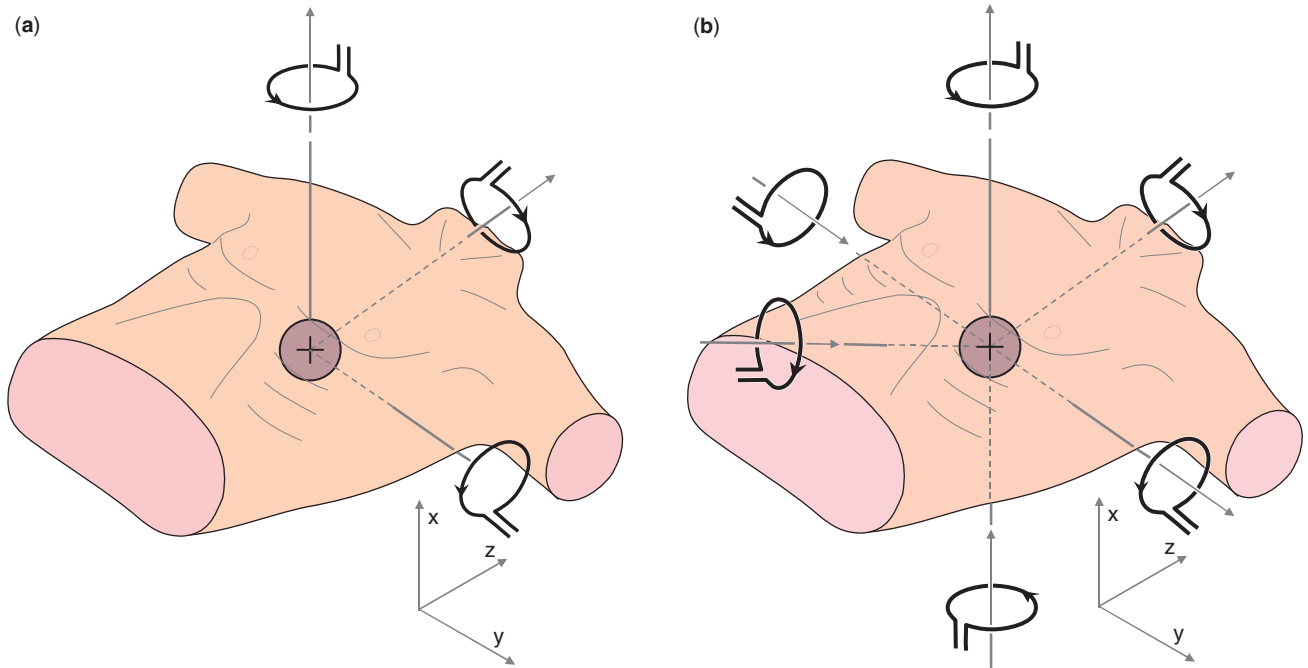
Figure 4. (a) The basic method for detecting the magnetic dipole moment of the heart, the *XYZ*-lead system. (b) Improvement of the lead fields of the *XYZ*-lead system by using bipolar measurements.

the VECG is very similar to the classical 12-lead ECG because most of the leads, except the precordial leads just in front of the cardiac muscle, detect the cardiac electric activity from so far that they include predominantly only a dipolar component of the source.

An attractive approach to increase the diagnostic performance of magnetocardiography is to use large number of leads and perform more accurate mapping of the cardiac magnetic field around the thorax. This method has also been applied to detecting the cardiac electric field. The mapping method includes the problem that when the measurements are made at a longer distance from the source, the signals recorded by adjacent leads include very similar information because their lead fields are
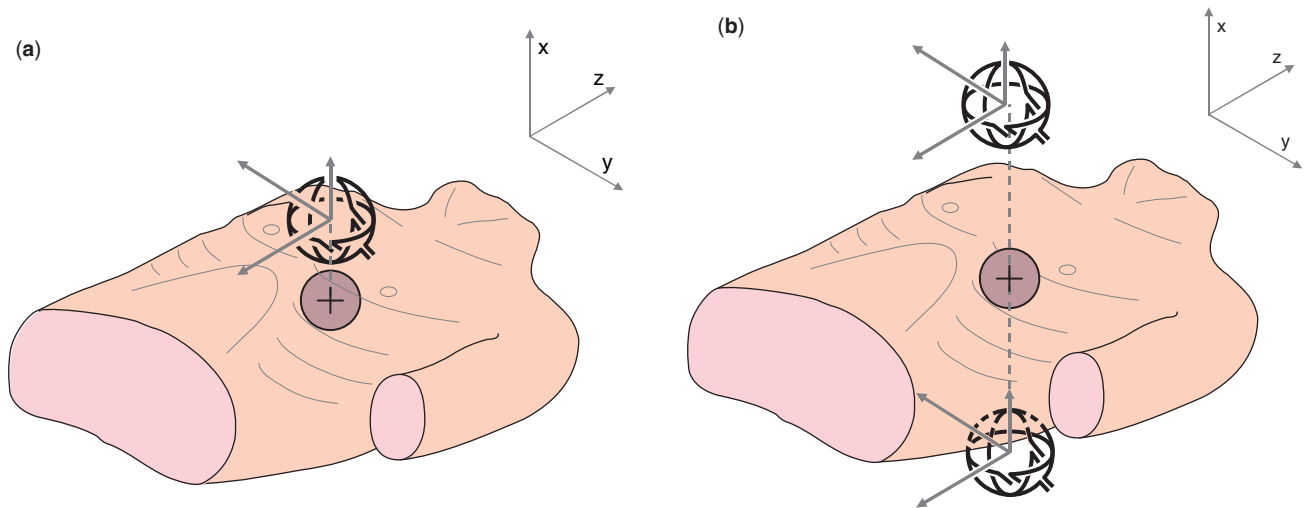
Figure 5. (a) The unipositional lead system. All the three components of the magnetic dipole are measured from single location. Note that the *Y*- and *Z*-components are measured in the negative direction and with double sensitivity. (b) The symmetric unipositional lead system. Similar measurements are made symmetrically on the anterior and posterior side at the same distance from the heart. (c) The dimensions and the lead field of the *X*-lead in the nonsymmetric unipositional lead system. The isosensitivity surfaces, shown with black lines, are calculated values. The region shaded with green is the HSV. The lead field, shown with blue lines, is everywhere oriented tangentially around the symmetry (coordinate) axis. (d) The dimensions and the lead field of the *X*-lead in the symmetric unipositional lead system. (e) The dimensions and the lead field of the *Z*-lead in the symmetric unipositional lead system. The lead field of the *Y*-lead is similar.
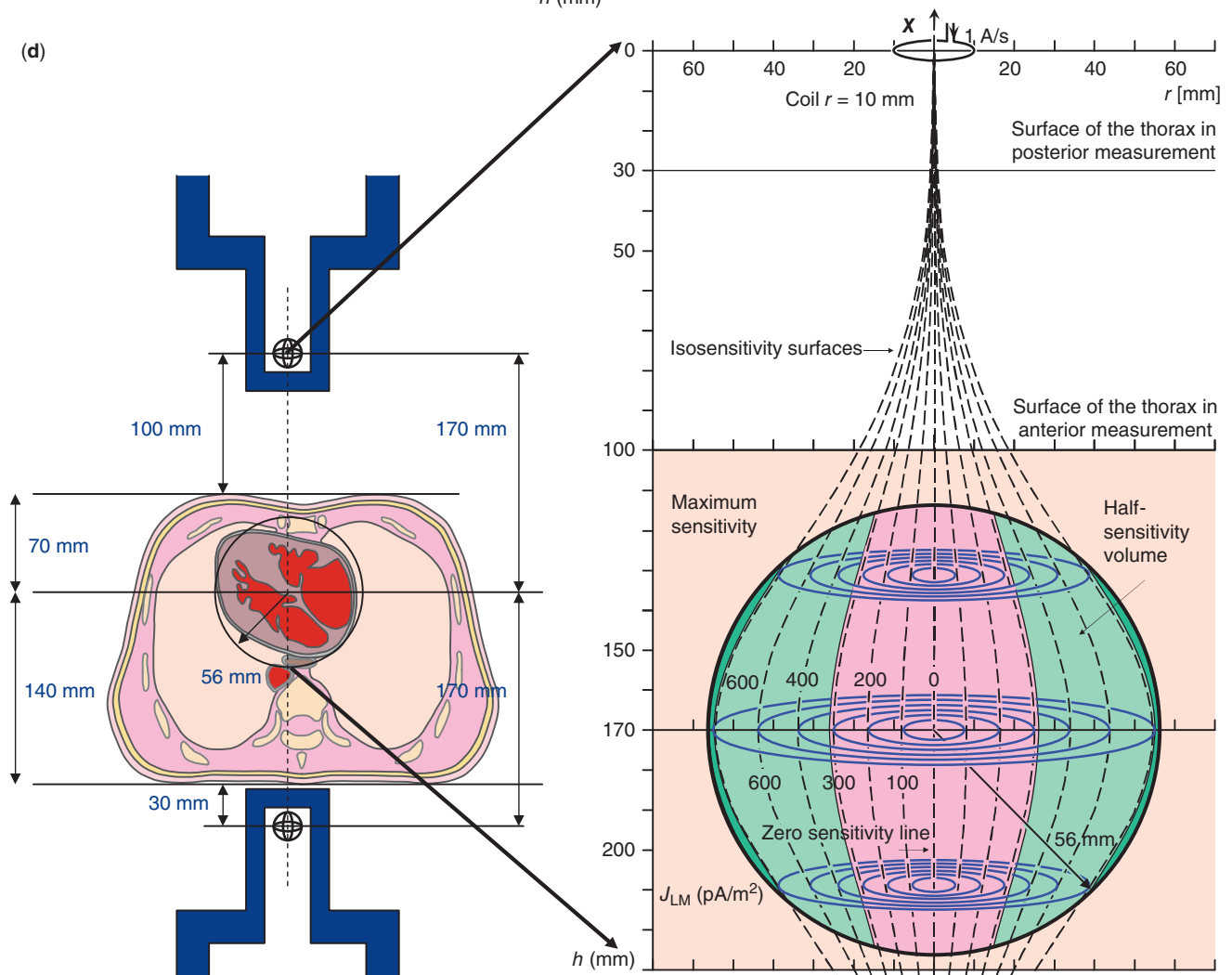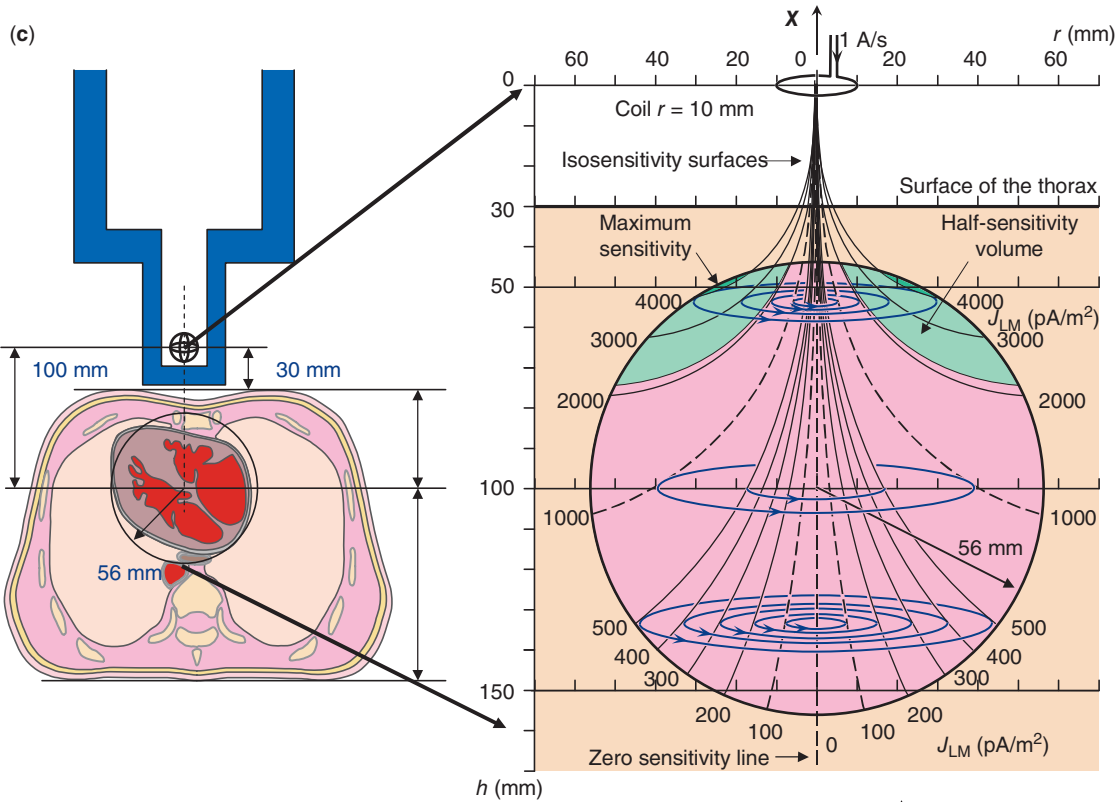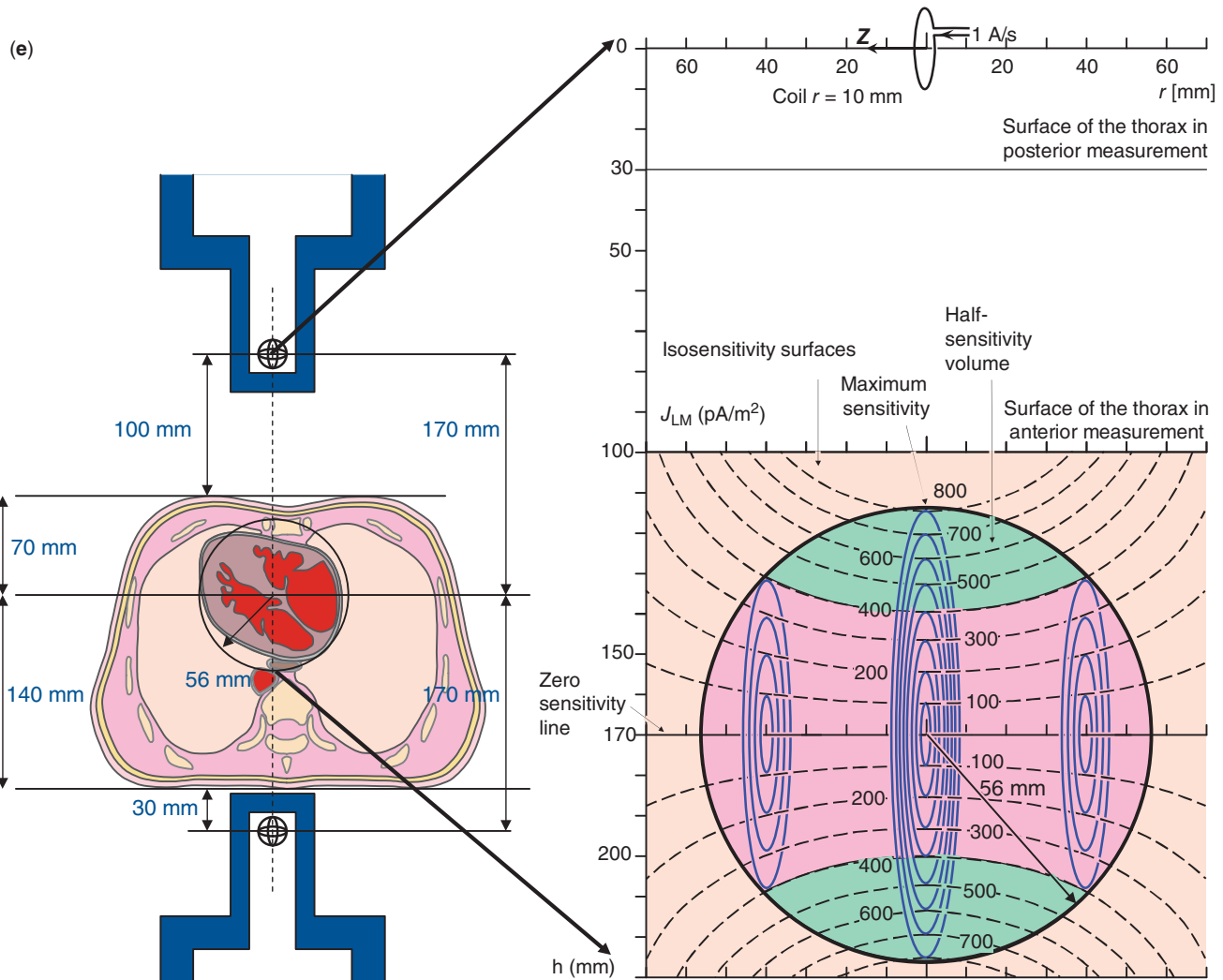
Figure 5. (*Continued*)

(e)

Figure 5. (*Continued*)

6.2. Theoretical Reasons to Use the MCG

very similar. This limits the mapping of the magnetic field to the anterior side of the thorax. Then also, the signal originates primarily from the anterior surface of the heart.

In mapping of the cardiac magnetic field typically a 64-channel axial gradiometer detector is used. From the detected magnetic field, it is possible to calculate the distribution of the electric current in the cardiac source for diagnostic purpose (23).

6.2. Theoretical Reasons to Use the MCG

It has been shown that MCG has clinical value and that it can be used either alone or in combination with ECG as a new technique called the *electromagnetocardio-gram* (EMCG). The diagnostic performance of the combined method is better than that of either ECG or MCG alone. With the combined method, the number of incorrectly diagnosed patients may be reduced by approximately 50%. This important issue is discussed in detail later.

6.3. Benefits and Drawbacks in the Application of the MCG

The technical differences between ECG and MCG include the MCG's far better ability to record sources down to DC, record sources on the posterior side of the heart, monitor the fetal heart, and perform electrodeless recording. As a technical drawback, it should be mentioned that the MCG instrument costs two to three times more than the ECG instrument. An important feature of MCG is that it does not necessarily need a magnetically shielded room. As will be discussed later, the MEG measurement is not possible to do without a shielded room. This is very important because the shielded room is not only very expensive, but it also limits the application of the technique to certain laboratory space.

7. MAGNETOENCEPHALOGAPHY

Similarly as in the cardiac applications, in the magnetic measurement of the electric activity of the brain, the

benefits and drawbacks of the MEG can be divided into theoretical and technical ones.

7.1. Bioelectromagnetic Properties

Sensitivity Distribution of the Axial Magnetometer. Calculation of the lead fields for magnetic leads is described in detail in References 16, 21, and 24. In a cylindrically symmetric volume conductor, the lead field flow lines are concentric circles and do not cut the discontinuity boundaries of the volume conductor. Therefore, the sensitivity distribution in the brain area of the spherical model equals that in an infinite, homogeneous volume conductor.

Figure 6a (16, 25, 27) illustrates the sensitivity distribution of an axial magnetometer with lead field current density vectors on a plane that is at the distance of one coil radius under the coil. Figure 6b illustrates the lead field of an axial magnetometer in the spherical head model of Rush and Driscoll (26). The blue lines circulating around the symmetry axis illustrate the lead field flow lines. Because the measurement sensitivity is linearly proportional to the distance from the symmetry axis, the sensitivity is zero on the symmetry axis. Therefore, the symmetry axis is in this case also the so-called *zero sensitivity line*. The black lines originating from the coil center join the points where the sensitivity has the same value, being thus so-called *isosensitivity surfaces*. The zero sensitivity line and the isosensitivity surfaces are for clarifying purpose drawn so that they continue from the model surface up to the coil level, although this is a hypothetical situation because no volume conductor exists in that region. But if they exist, the lines would look like this. The region shaded with green represents the HSV. The concept of zero sensitivity line is shown more accurately in Figure 6c. Please note that the skull resistivity does not have any effect to MEG lead fields, but it is essential in comparing the properties of MEG and EEG.

Sensitivity Distribution of the Planar Gradiometer. The lead fields for planar gradiometers are simply obtained by superposition of the lead fields for each separate coil (16, 25, 26). Figure 7a on the left illustrates the sensitivity distribution of a planar gradiometer with lead field current density vectors on a plane that is in the distance of one coil radius under the coil. Please note that the lead field has very linear orientation in the region between the coils, where the sensitivity is the highest. This distribution resembles the sensitivity of a bipolar electric lead as shown in Figure 7a on the right. Figure 7b illustrates the lead field of a planar gradiometer in the spherical head model of Rush and Driscoll (26). The blue lines circulating around the symmetry axis illustrate the lead field flow lines, and the black lines originating from the centers of the coils represent the isosensitivity surfaces. The region shaded with green color represents the HSV. Furthermore, the zero sensitivity line begins from one coil and ends to the other coil forming a loop in the volume conductor area.

The lead fields for axial and planar gradiometers are shown for the whole brain area of the model, though the relevant measurement region is only the HSV. and its vicinity. In the region of the brain opposite to the coils, the measurement sensitivity is so low that the signal recorded from that region is well shadowed by the stronger signal from the HSV region and not detected.

HSVs in EEG and MEG. The HSVs are calculated for two- and three-electrode EEG leads and for axial and planar gradiometer MEG leads as a function of electrode distances and gradiometer baselines as shown in Figure 8. The calculation results are shown in Figure 9. The resistivity ratio for skull/brain in the model is 80/1. The minimum HSV is, of course, achieved with the shortest distance/baseline. For two- and three-electrode EEG leads, the HSVs at $1°$ electrode distance (1.6 mm) are 1.2 and $0.2 \, cm^3$, respectively. For 10 mm radius planar and axial gradiometer MEG leads, these volumes at $1°$ of coil separation (that is 1.6 mm baseline for axial gradiometer) are 3.4 and $21.8 \, cm^3$, respectively. The effect of the skull resistivity to the HSV is shown in Figure 10 (28). The skull/brain resistivity ratio 80/1, first published by Rush and Driscoll in 1969 (26), was not based on any extensive study because the main purpose of that article was to introduce the calculation of the EEG lead fields. Despite that it was used by the scientific community over 30 years. The skull resistivity was examined carefully in the beginning of this century in two publications (29, 30). On the basis of these data for the resistivity ratio, nowadays a value around 10/1 is used.

The 10 mm coil radius and 20 mm coil distance from scalp are realistic for the helmet-like whole-head MEG detector. There exist, however, MEG devices for recording at a limited region where the coil distance and the coil radii are of the order of 1 mm. Therefore, the HSVs for planar gradiometers with 1 mm coil radius at 0–20 mm recording distances are also illustrated in Figure 11. These curves show that when the MEG recording distance h is about 12 mm and the EEG electrode distance/ MEG gradiometer baseline is 1.6 mm, the planar gradiometer has about the same HSVs as the two-electrode EEG.

Short separation will, of course, also decrease the signal amplitude. An optimal value is about $10°$ (16 mm) separation. This decreases the EEG and MEG signal amplitudes to approximately 70–80% of their maximum value, but the HSVs do not increase considerably from their values at $1°$ of separation (25).

Thus, contrary to general belief, the EEG does not have worse ability to focus its sensitivity to a small region in the brain than the whole-head MEG. The sensitivity distributions of these leads are, however, very similar. Note that if the sensitivity distributions of two different lead systems are the same, whether they are electric or magnetic ones, they detect the same source and produce the same signal. Therefore, the planar gradiometer and two-electrode EEG lead detect very similar source distributions.

Sensitivity of EEG and MEG to Radial and Tangential Sources. The three-electrode EEG has its maximum sensitivity under the central electrode. This sensitivity is mainly
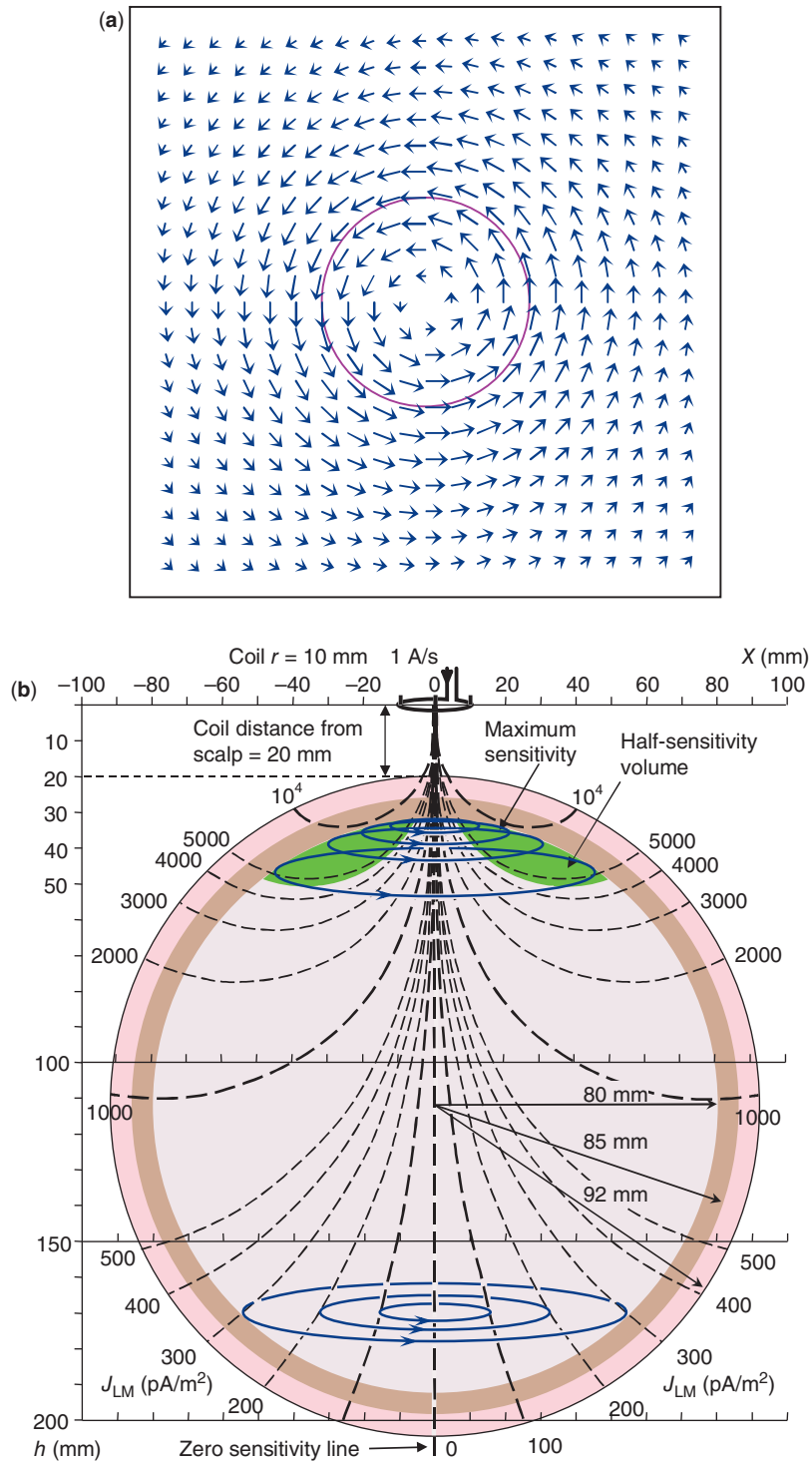
Figure 6. (a) The lead field (sensitivity distribution) of a magnetometer coil on a plane at the distance of the coil radius. The lead field is shown with calculated current density vectors. The coil is illustrated with the red circle. (Reprinted with permission from Ref. 3. Copyright 2012, Springer Science+Business Media, LLC.) (b) The lead field (sensitivity distribution) of an axial magnetometer in the inhomogeneous spherical head model. The calculated isosensitivity surfaces are shown with black dashed lines. The coil radius is 10 mm and its distance from the scalp is 20 mm. (c) If the magnetometer coil axis coincides with the symmetry axis of a spherically symmetric head model, this axis is the zero sensitivity line. Therefore, an electric source locating on this axis generates no signal to the magnetometer. (Reprinted with permission from Ref. 3. Copyright 2012, Springer Science+Business Media, LLC.)
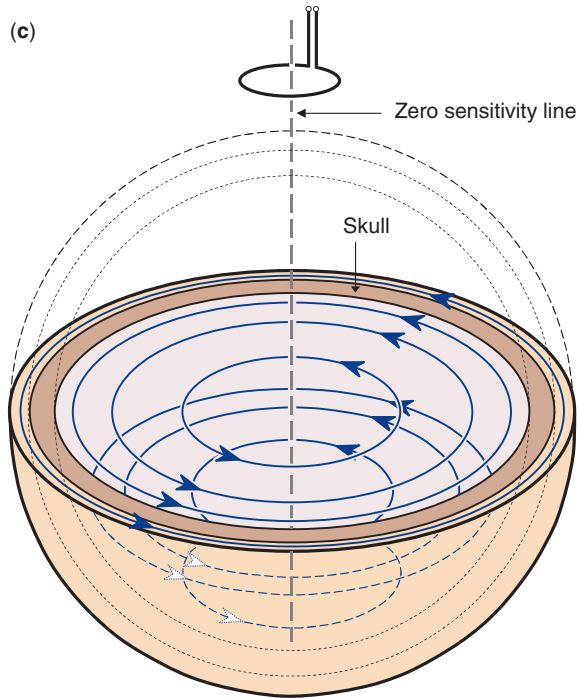
Figure 6. (*Continued*)

directed radially to the spherical head model. With short electrode distances, the sensitivity of the two-electrode EEG ismainly directed tangentially to the spherical head model. Thus, with the EEG it is possible to detect sources in all three orthogonal directions, that is, in the radial and in the two tangential directions, in relation to the spherical model, Figure 8.

In the axial gradiometer MEG lead, the sensitivity is directed tangentially to the gradiometer symmetry axis and thus also tangentially to the spherical head model. In the planar gradiometer, the sensitivity has its maximum under the middle of the coils and is directed tangentially and mainly linearly to the spherical head model. Thus, the MEG lead fields are oriented tangentially to the spherical head model everywhere. This may be easily understood by recognizing that the lead field current cannot flow through the surface of the head because no electrodes are used. Therefore, the MEG can only detect sources oriented in the two tangential directions in relation to the spherical model, Figure 8.

7.2. Theoretical Reasons to Use the MEG

Because the skull is transparent for magnetic field and the head may be well modeled with a spherical model, the MEG lead fields are not affected by the inhomogeneities of the head. For these reasons in the beginning of biomagnetic research it was believed that the MEG should be able to concentrate its measurement sensitivity in a smaller region than the EEG. This issue is discussed in the following. The analysis is made using the classic spherical head model introduced by Rush and Driscoll (26). In this model, the head is represented with three concentric spheres, where the outer radii of the scalp, skull, and brain are 92, 85, and 80 mm, respectively. The resistivities of the scalp and the brain are 2.22 Ωm and that of the skull is 80 times higher, being 177 Ωm.
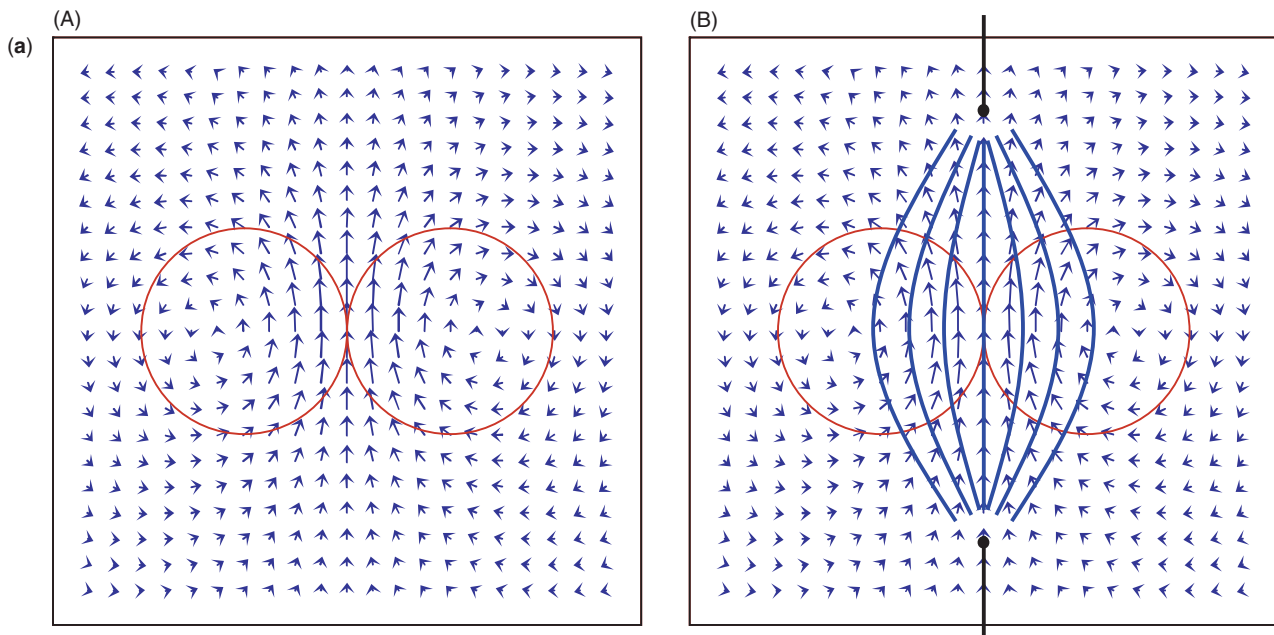
Figure 7. (a) Part (A): The calculated lead field of a planar gradiometer on a plane at the distance of the coil radius from the coils which are illustrated with the red circles. Note that the lead field is mainly linear in the middle of the coils. Part (B): The lead field of a planar gradiometer resembles that of a bipolar electric lead. It is sketched with the blue lines. (Reprinted with permission from Ref. 3. Copyright 2012, Springer Science+Business Media, LLC.) (b) The lead field of a planar gradiometer in the inhomogeneous spherical head model. The coil radii are 10 mm with a baseline of 20 mm and distance from scalp 20 mm. The calculated isosensitivity surfaces are shown with black dashed lines. The blue lead field flow lines are sketched.

(b) Planar gradiometer coils r = 10 mm   1 A/s X (mm)

Coil distance from scalp = 20 mm

Maximum sensitivity

Half-sensitivity volume

Zero sensitivity line

J_{LM} (pA/m²)

h (mm)

Figure 7. (*Continued*)

2 electrodes

1+2 electrodes

r = 10 mm   20 mm

Axial gradiometer

r = 10 mm   20 mm
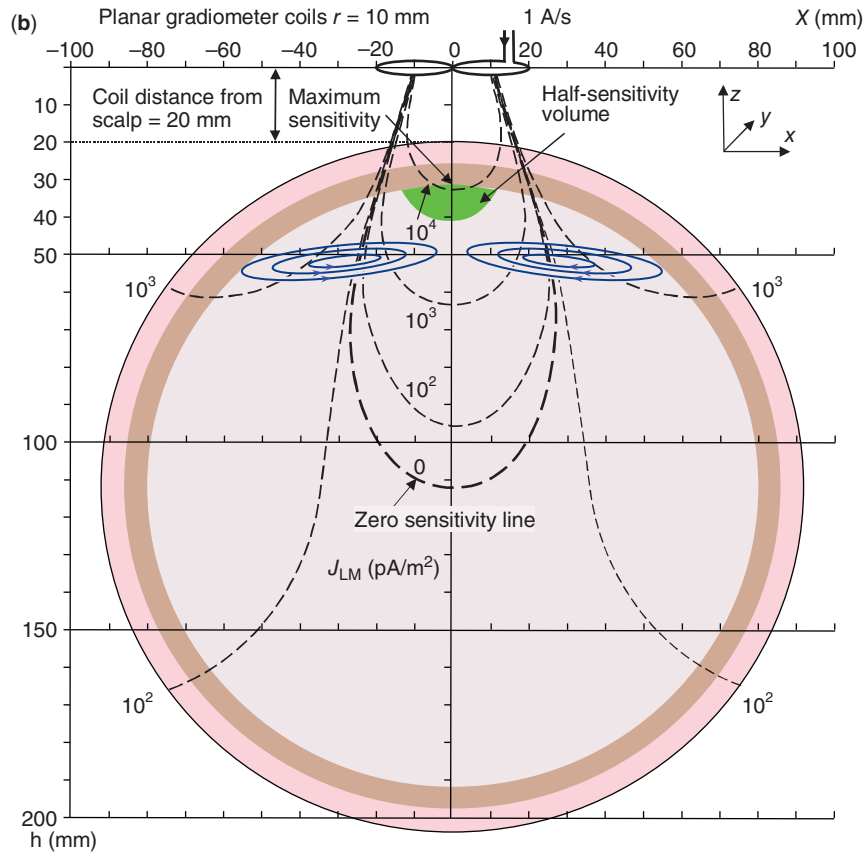
Planar gradiometer
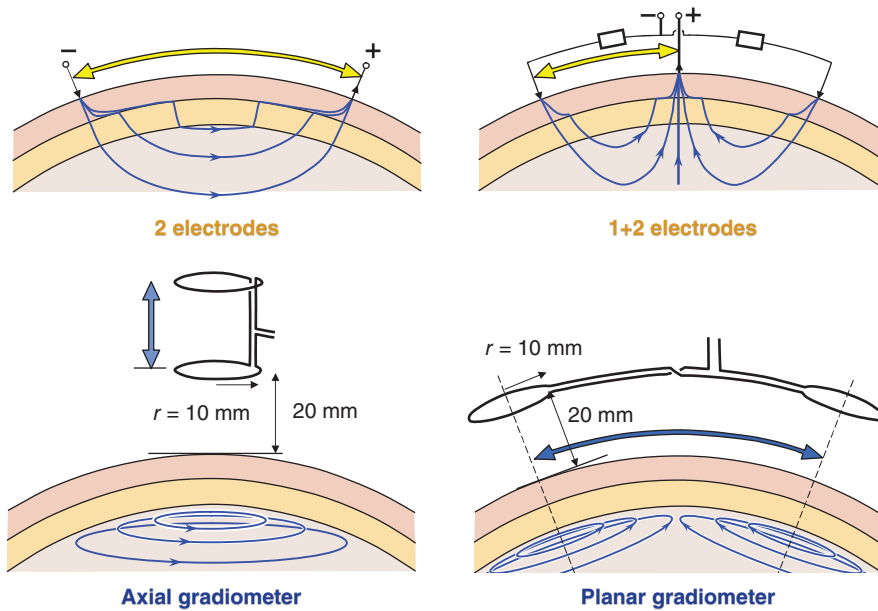
Figure 8. Description of the HSV calculations for two- and three-electrode EEG leads (upper row) and for axial and planar gradiometer MEG leads (lower row) as a function of electrode distance and coil separation, respectively, for the Figures 9–11.
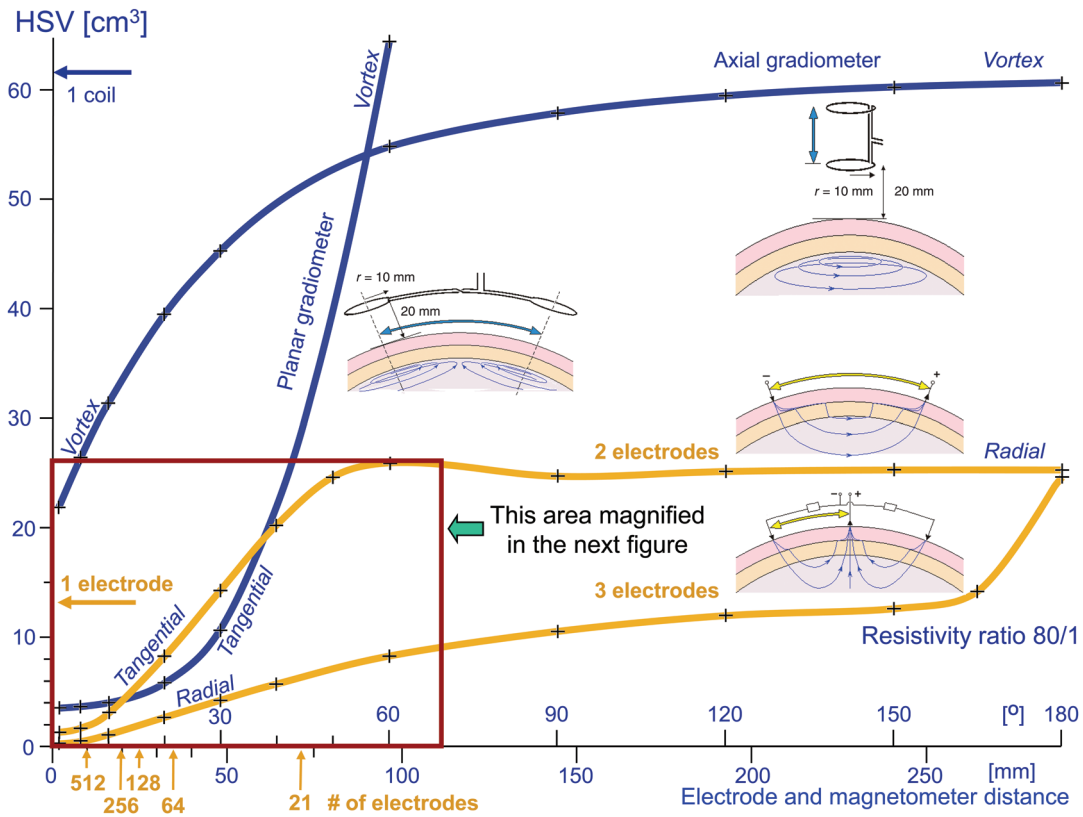
Figure 9. The calculated HSVs (y-axis) of different EEG (orange) and MEG (blue) leads in the Rush-Driscoll spherical head model as a function of electrode distance and magnetometer baseline, respectively. The electrode and magnetometer distances (x-axis) are shown both in degrees and in millimeters. 80/1. The inner sphere volume is 2145 cm³.
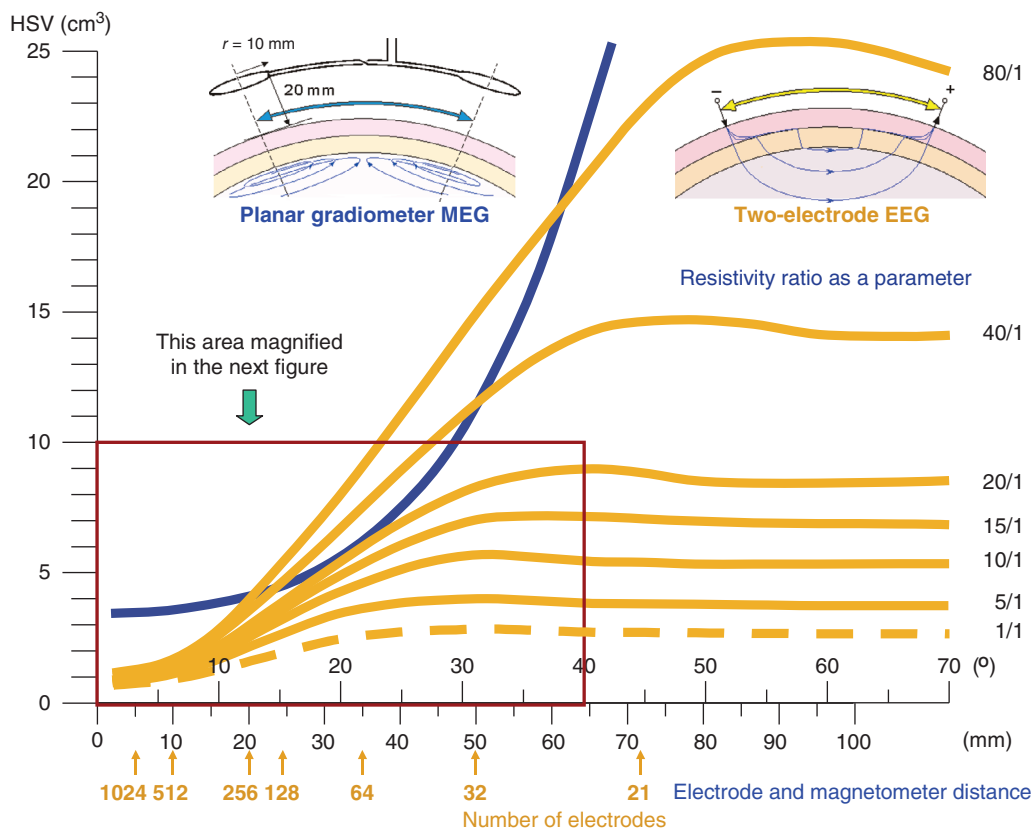
Figure 10. The lower left corner of the previous figure magnified. The HSVs are calculated for EEG with different skull/brain resistivity ratios. The high resistivity of the skull does not have any effect to the MEG measurement.
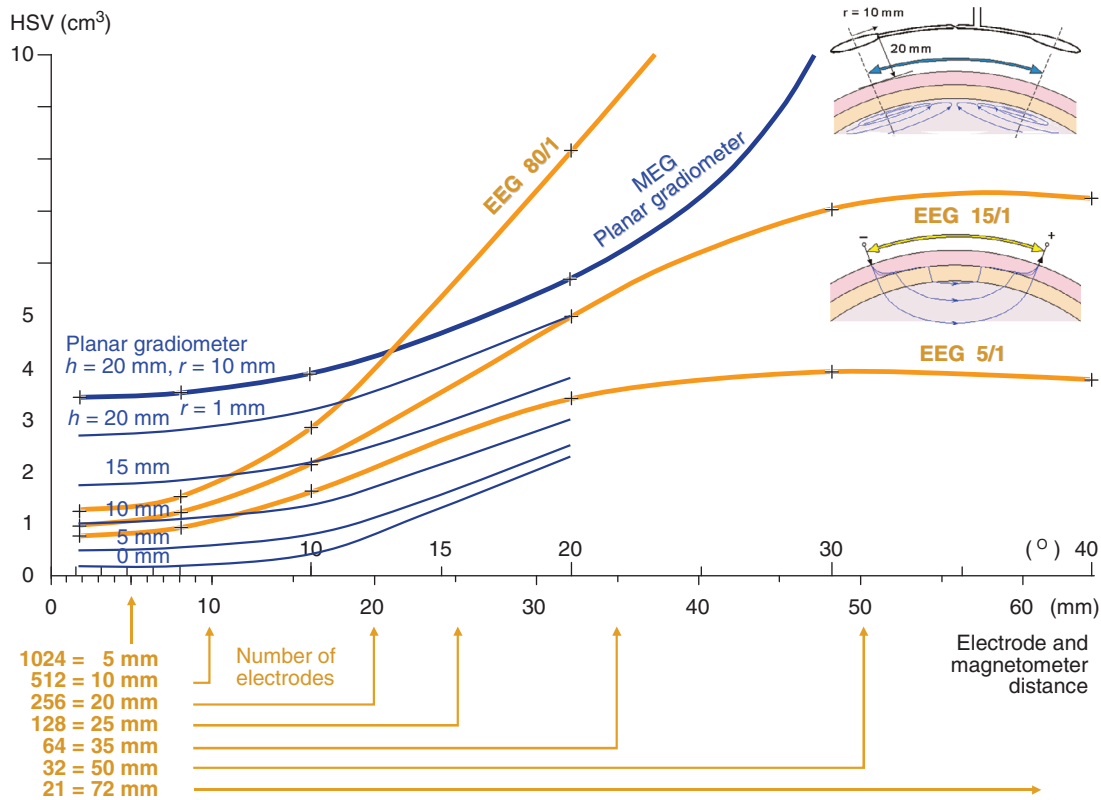
Figure 11. The lower left corner of the previous figure magnified. It is shown the calculated HSV (blue lines) for a planar gradiometer with the coil radius of 1 mm and with different coil distances from scalp as a function of the gradiometer baseline. The half-sensitivity volume is also shown for bipolar EEG with different skull resistivity ratios. It is also shown the distances of EEG electrodes in different EEG-lead systems with different number of electrodes.

The two basic magnetometer constructions that are used in MEG are axial and planar gradiometers. In the former one, the coils are coaxial, and in the latter one, they are coplanar. The minimum distance of the coil from the scalp in a superconducting magnetometer is about 20 mm. The coil radius is usually about 10 mm. It has been shown (16, 21, 24) that with this measurement distance, decreasing the coil radius does not change the distribution of the sensitivity in the brain region. In the following, the sensitivity distribution of these gradiometer constructions is discussed in detail.

In MCG it is usually detected the magnetic dipole moment of the volume source of the heart. In MEG, however, the primary purpose is to detect the electric activity of the cortex and to localize the regions of certain activity. Therefore, good spatial resolution in MEG has important value.

7.3. Benefits and Drawbacks in the Application of the MEG

The technical differences between EEG and MEG also include the MEG's far better ability to record sources down to DC. Another benefit is that MEG does not need fixing electrodes, which is an advantage in multi-channel systems having 250 or more channels. On the other hand, the patient needs to hold the head in a static position that is stressing in long recording sessions. As a technical drawback, it should be mentioned that the MEG instrument costs perhaps 100 times more than the EEG instrumentation with the same number of channels. Another important feature of MEG is also that it needs a heavy magnetically shielded room that also limits the application of the technique to certain laboratory space.

8. INDEPENDENCE OF BIOELECTRIC AND BIOMAGNETIC FIELDS

Central issue in the discussion on biomagnetism is the independence of the bioelectric and biomagnetic fields: Are they independent fully, partially, or at all? If the fields are not independent, the use of biomagnetism in addition to bioelectricity does not improve the diagnosis of diseases. If they are fully, or at least partially independent, it improves the diagnosis. In the beginning of biomagnetism research, there were two published important publications on this issue written by Robert Plonsey (31) and Stanley Rush (32). They came to fully opposite conclusion on this issue. In the following, this fundamental problem of independence is

discussed and also how the opposite conclusions of Plonsey and Rush actually complement each other.

Let us first discuss this issue on the basis of the Helmholtz theorem. Helmholtz theorem states that (33, 34): "A general vector field which vanishes at infinity can be represented as a sum of two independent vector fields, one that is irrotational (zero curl) and another which is solenoidal (zero divergence)." The bioelectric source, that is, the impressed current source, may be divided into two components that are called the flux and the vortex sources:

$$\boldsymbol{J}^{\mathrm{i}} = \boldsymbol{J}^{\mathrm{i}}_{\mathrm{F}} + \boldsymbol{J}^{\mathrm{i}}_{\mathrm{V}} \tag{10}$$

If we observe the equations of the sources of bioelectric and biomagnetic fields (16):

$$\boldsymbol{J}^{\mathrm{i}}_{\mathrm{F}} = -\nabla \cdot \boldsymbol{J}^{\mathrm{i}}, \qquad V_{\mathrm{LE}} = \int_v \Phi_{\mathrm{LE}} \nabla \cdot \boldsymbol{J}^{\mathrm{i}} \mathrm{d}v \tag{11a, b}$$

where Φ_{LE} is the electric scalar potential due to reciprocal energization of the electric lead, that is, feeding a unit current to the lead (16). The quantity $-\nabla \cdot \boldsymbol{J}^{\mathrm{i}} \mathrm{d}v$ is the strength of the impressed current source and is defined as the *flow* (or *flux*) *source* I_{F}.

$$\boldsymbol{J}^{\mathrm{i}}_{\mathrm{V}} = -\sigma \nabla \times \boldsymbol{J}^{\mathrm{i}}, \qquad V_{\mathrm{LM}} = (\mu/2) \int_v \Phi_{\mathrm{LM}} \boldsymbol{r} \cdot \nabla \times \boldsymbol{J}^{\mathrm{i}} \cdot \mathrm{d}v$$

$$\tag{12a, b}$$

where Φ_{LM} is the magnetic scalar potential due to reciprocal energization of the magnetic lead. The quantity $\nabla \times \boldsymbol{J}^{\mathrm{i}}$ is defined as the *vortex source* I_{v}. Now we see that the bioelectric fields rise from the flux source and the biomagnetic fields from the vortex source.

Based on this, Plonsey came to the conclusion that "Since the flux and vortex sources are independent, ECG and MCG are similarly independent" (31). Stanley Rush concluded on the basis of the Maxwell's equations that "The independence of the flow and vortex sources is only a mathematical possibility. The flow and vortex sources are one-to-one with each other" (32).

This fundamental controversy confused the biomagnetic community over 20 years before it was solved by Jaakko Malmivuo in 1995 (16). He found, on the basis of the lead field theory, that the source distributions, that is, the lead fields of bioelectric and biomagnetic measurements, are independent. However, the bioelectric and biomagnetic fields are only partially independent. This may be demonstrated in the following way. Let us discuss it on the dipolar level.

The electric dipole moment of the volume source, that is, vector electrocardiogram, VECG, is detected with a detector, whose lead field is composed of three orthogonal components, each being homogeneous and linear in the directions of the coordinate axes (Figure 2) (16, 21). These are independent of each other, that is, it is not possible to synthesize one of them as a linear combination of the two other ones.

The magnetic dipole moment of the volume source, that is, vector magnetocardiogram, VMCG, is detected with a detector, whose lead field is also composed of three orthogonal components, each being tangential around corresponding coordinate axis. The magnitude of the sensitivity is proportional to the radial distance from the symmetry axis (Figure 3) (16, 21). Also, these are independent of each other, that is, it is not possible to synthesize one of them as a linear combination of the two other ones.

On the basis of the Helmholtz theorem, these electric and magnetic *lead fields* are mutually independent. Therefore, none of the six components of the electric and magnetic lead fields is a linear combination of the other five.

Although the electric and magnetic lead fields are orthogonal, that is, independent, the recorded *signals are not fully independent*. Let us discuss this with the following example. When having bipolar electric and magnetic leads, whose symmetry axes coincide, their lead fields are orthogonal everywhere in the volume conductor (Figure 12). (Based on this situation, in the beginning of biomagnetic research it was believed that electric and magnetic
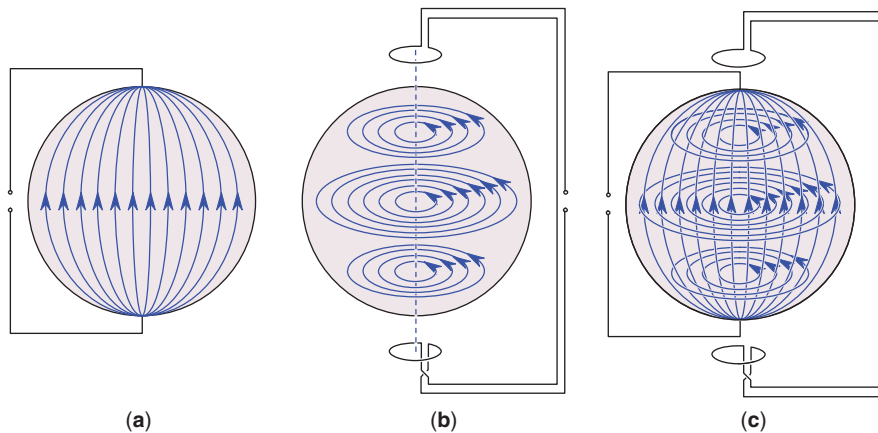
Figure 12. (a) Bipolar EEG lead field in a homogeneous spherical head model (sketched). (b) Bipolar MEG-lead field in a homogeneous spherical head model. (c) The aforementioned lead fields are orthogonal everywhere in the head model. (Reprinted with permission from Ref. 3. Copyright 2012, Springer Science+Business Media, LLC.)
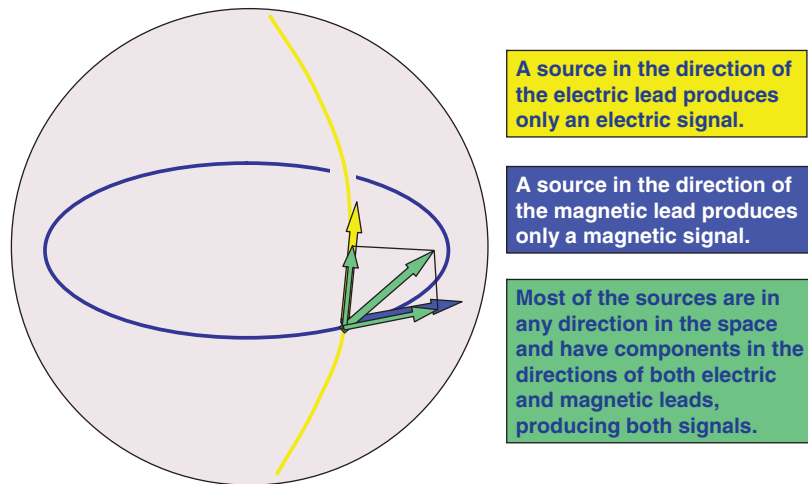
Figure 13. Although the electric and magnetic lead fields in the configuration of the previous figure are orthogonal throughout the spherical model, the recorded EEG and MEG signals are only partially independent. See the text for more details. (Reprinted with permission from Ref. 3. Copyright 2012, Springer Science+Business Media, LLC.)

measurements are complementary, that is, recording fully independent information. As we see here, this conclusion was, however, wrong.) If there is a current source element in the direction of the electric lead field, it generates a signal to the electric lead, but no signal to the magnetic lead. Similarly, if there is a current source element in the direction of the magnetic lead, it generates a signal to the magnetic lead, but no signal to the electric lead. Despite this, the electric and magnetic signals are not fully independent, since most of the current source elements are oriented in any direction in the space and having a component both in the direction of the electric lead and the magnetic lead (Figure 13) (3, 35–37).

On the basis of the Maxwell's equations, if we know the *total* electric field, outside and inside the volume source, we should be able to calculate the corresponding magnetic field. In this situation recording the magnetic field does not bring independent information. However, recording the total electric field is not possible and in practice it is only recorded its dipolar component. From this it is not possible to calculate the dipolar component of the magnetic field. Therefore, recording the dipolar magnetic field in addition to the electric field brings additional information of the source.

On the other hand, if the sensitivity distributions of two detection methods – regardless of whether they are electric or magnetic – are identical in the source region, the signals and their information contents are also identical.

9. DIAGNOSTIC PERFORMANCE OF BIOELECTRIC AND BIOMAGNETIC METHODS

There are two notable studies on the diagnostic performance of bioelectric and biomagnetic methods. One of them is on ECG/MCG (3, 37, 38), and the other one is on EEG/MEG (39). In brief, both of them came to similar conclusion: The electric and magnetic methods are on average equally capable in diagnosis. Combining these methods increases the joint diagnostic performance. That, however, is not the sum of the capabilities of the electric and the magnetic methods.
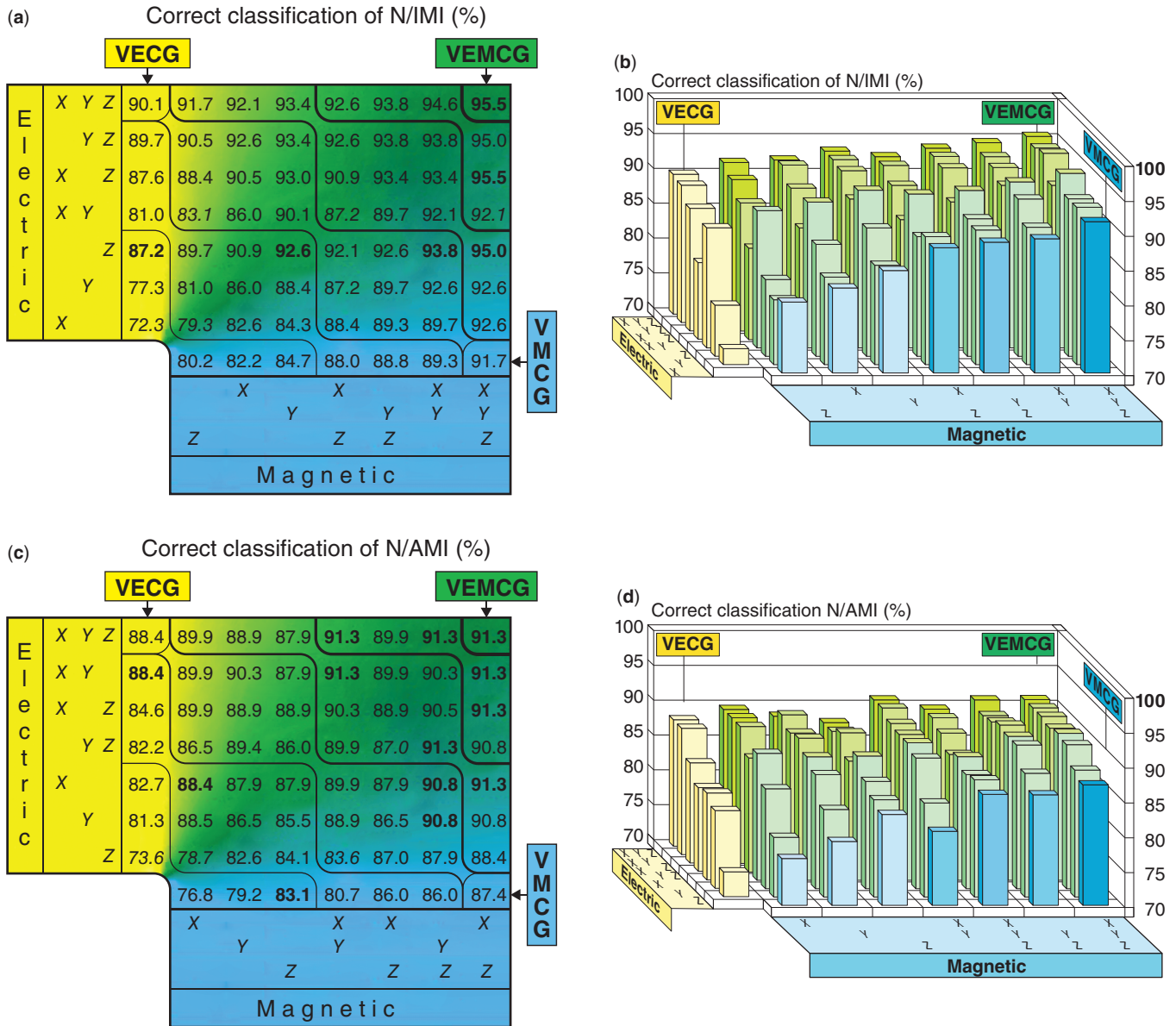
9.1. Comparison of the ECG and the MCG

The diagnostic performance of ECG and MCG was compared in an extensive study made at the Ragnar Granit Institute (3, 37, 38). The study was made using the non-symmetric unipositional lead system, that is, making the measurements only on the anterior side of the thorax. The patient material was, however, selected so that myocardial changes were located dominantly on the anterior side.

We have large material of MCG recordings consisting of 290 normal subjects and 259 patients with different myocardial disorders (36). From this material, 90 patients with old inferior myocardial infarction (IMI), 71 patients with old anterior myocardial infarction (AMI), and 152 normal healthy subjects were selected. Thus, the total number of subjects in the study was 313. The selection to these groups was made with nonelectromagnetic methods. This is the first large-scale statistically relevant study of the clinical diagnostic performance of biomagnetism.

First, it was calculated the correct jackknifed classification rates (%) (39) in linear discriminant analysis (LDA) between normals and patients with inferior myocardial infarction (N/IMI). This was made for all combinations of dipolar electric and magnetic leads from single leads up to six leads. The results are presented in increasing order in Figure 14a. VECG shown on the top of the first electric column (yellow) has the value of 90.1%. VMCG shown on the right of the lowest magnetic row (blue) has the value of 91.7%. Their combination, vector electromagnetocardiography (VEMCG), shown in the top right corner (green) has the value of 95.5%. The same results are also shown in a graphical presentation (Figure 14b).

Figures 14c and d show similarly calculated data between normals and patients with anterior myocardial infarction (N/AMI). Note that the N/AMI data behave in similar way as the N/IMI data, except that the order of sensitivity for both the electric and the magnetic leads is

(a) Correct classification of N/IMI (%)

Electric	VECG							VEMCG
X Y Z	90.1	91.7	92.1	93.4	92.6	93.8	94.6	**95.5**
Y Z	89.7	90.5	92.6	93.4	92.6	93.8	93.8	95.0
X Z	87.6	88.4	90.5	93.0	90.9	93.4	93.4	**95.5**
X Y	81.0	*83.1*	86.0	90.1	*87.2*	89.7	92.1	*92.1*
Z	**87.2**	89.7	90.9	**92.6**	92.1	92.6	**93.8**	**95.0**
Y	77.3	81.0	86.0	88.4	87.2	89.7	92.6	92.6
X	72.3	*79.3*	82.6	84.3	88.4	89.3	89.7	*92.6*
VMCG	80.2	82.2	84.7	88.0	88.8	89.3	91.7	

Magnetic: X / Y / Z combinations

(b) Correct classification of N/IMI (%) (VECG, VEMCG, VMCG — graphical 3D bar form; axes Electric, Magnetic, 70–100)

(c) Correct classification of N/AMI (%)

Electric	VECG							VEMCG
X Y Z	88.4	89.9	88.9	87.9	**91.3**	89.9	**91.3**	**91.3**
X Y	**88.4**	89.9	90.3	87.9	**91.3**	89.9	90.3	**91.3**
X Z	84.6	89.9	88.9	88.9	90.3	88.9	90.5	**91.3**
Y Z	82.2	86.5	89.4	86.0	89.9	*87.0*	**91.3**	90.8
X	82.7	**88.4**	87.9	87.9	89.9	87.9	**90.8**	**91.3**
Y	81.3	88.5	86.5	85.5	88.9	86.5	**90.8**	90.8
Z	73.6	78.7	82.6	84.1	*83.6*	87.0	87.9	88.4
VMCG	76.8	79.2	**83.1**	80.7	86.0	86.0	87.4	

Magnetic: X / Y / Z combinations

(d) Correct classification N/AMI (%) (VECG, VEMCG, VMCG — graphical 3D bar form; axes Electric, Magnetic, 70–100)

Figure 14. (a) Correct classification (%) between normal subjects (N) and patients with old inferior myocardial infarction (IMI) when using different number (1, . . . , 6) of dipolar electric and magnetic leads in the diagnostic system. (b) The data of part (a) shown in graphical form. From here it is more clearly seen that the correct classification rate increases as a function of number of leads independently whether the used leads are electric or magnetic ones. (c and d) Similar data as in parts (a) and (b) between normal subjects (N) and patients with old anterior myocardial infarction (AMI), respectively.

different. This is, therefore, that due to the different location of the abnormal tissue, different leads are more sensitive to detect it. Please note also that the correct classification rates of the electric (VECG) and magnetic (VMCG) leads in classifying N/IMI and N/AMI are about equally good and that the classification rate of their combination (VEMCG) is bigger than either of the aforementioned. It is not (and can not be) as big as the sum of the aforementioned. This is therefore that the patient groups classified correctly with either method are partially overlapping (Figure 15).

Conclusions. From this data it is possible to make some important conclusions:

1. The correct classification rates of VECG and VMCG for N/IMI, being 90.1 and 91.7%, respectively, are about equal. This means that ECG and MCG have about the same diagnostic performance (Figures 14a and b).

2. The diagnostic parameters in N/IMI were then selected from both ECG and MCG. This combined method is called electromagnetocardiogram, EMCG.
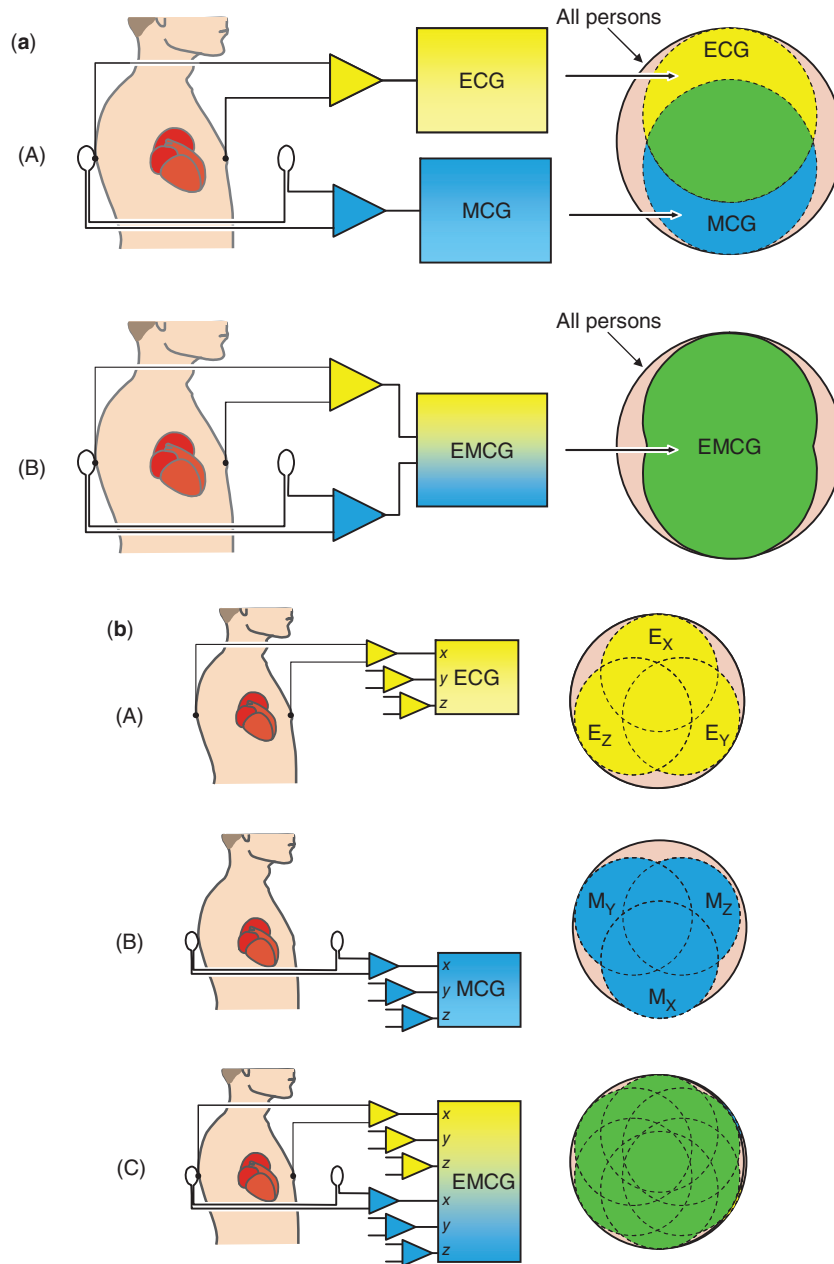
Figure 15. (a) Improvement of the diagnostic performance by combining ECG and MCG to EMCG. (b) This principle is not new. Just the same principle holds within the three electric leads as well as within the three magnetic leads.

With the EMCG the classification rate was 95.5%. The improvement, 5% units, sounds small, but the improvement is statistically significant ($p=0.019$). This also means that the number of incorrectly diagnosed patients decreased from 9.9 to 4.5%, that is, to one half, which is important. This improvement in diagnostic performance was obtained without increasing the number of parameters used in the diagnostic procedure (38). (Please note that the diagnostic performances are quite high because the diagnostic question was simple: Does the patient have IMI or not?)

3. The behavior of the data recorded from the patients with old anterior myocardial infarction (N/AMI) behaves similarly as that for the patients with old inferior myocardial infarction (N/IMI) (Figures 14a and c, 14b and d). Only the order of sensitivity for the leads is different.

4. The patient groups, which were classified correctly with ECG and MCG, are about the same size but they are not the same groups. They are partially overlapping (Figure 15).

5. This finding is not new. The same principle exists also within the three VECG leads and within the

three VMCG leads, respectively. The classification rates for single VECG leads for N/IMI are 72.3, 77.3, and 87.2% for the leads *X*, *Y*, and *Z*, respectively. The classification rate when using all the three VECG leads is 90.1%, which is less than the sum of the classification rates of each single lead. Thus, the patient groups classified correctly with each of the three VECG leads are also overlapping (part A in Figure 15b). The situation is similar with the three VMCG leads, whose classification rates are 80.2, 82.2, and 84.7% for the *Z*, *X*, and *Y* leads, respectively. Although the groups of correctly diagnosed subjects of both methods are about equal in size, the groups are not identical and not separate either, but they are partially overlapping. Combining them to EMCG improves the diagnostic performance (part C in Figure 15b). The diagnostic performance may increase even so much that the number of incorrectly diagnosed patients may be decreased to half.

6. The behavior of the diagnostic performance is similar with the patients with anterior myocardial infarction (AMI) (Figure 14c). The main difference is that the order of superiority of the electric and magnetic leads is different from that with IMI because the location of the abnormality in the cardiac muscle is different.

7. The classification rate improves as a function of number of component leads independently whether they are electric or magnetic ones. This is clearly seen in Figure 14b, where the data of Figure 14a are illustrated in graphical form.

8. It may be anticipated that when taking the average of the results from a large number of similar diagnostic studies with various diseases, this improvement as a function of number of electric and magnetic leads will be very smooth.

9. The aforementioned behavior means that all the six dipolar electric and magnetic leads are on average of the same value and taking more and more of them to the diagnostic system improves the diagnostic performance of the system. However, the amount of improvement decreases when more and more of the leads already exist in the system (Figure 16).

10. These studies confirm that the electric and magnetic leads are elements of the family of electromagnetic leads making them all equally good on average.

11. In addition, the electric and magnetic leads have some specific properties that are discussed later.

9.2. Comparison of the EEG and the MEG

Iwasaki et al. (40) published in 2005 a study where they made a blinded comparison of EEG and MEG in detecting epileptic spikes. They recorded the EEG with the standard 10–20 system including 23 electrodes. The MEG recordings they made were of part of the patients with a 122 channel MEG system and part of them with a 204 channel MEG
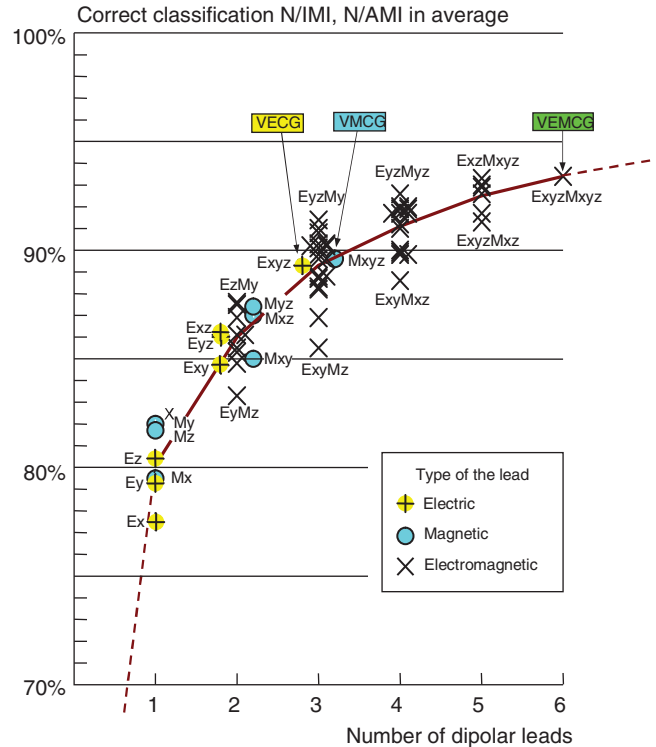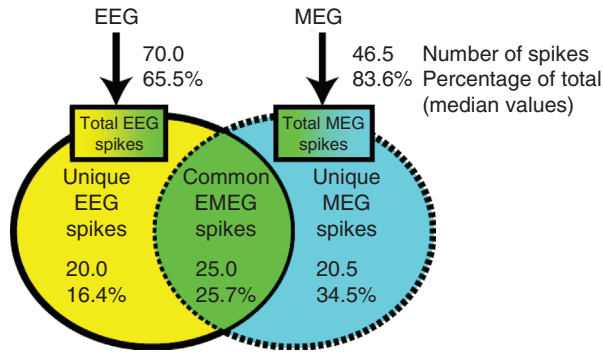

Figure 16. Correct classification of N/IMI and N/AMI is presented on average for each lead combination. It is seen, that the additional improvement in the correct classification due to an added lead becomes the smaller the more there already are leads in the diagnostic system. The average values of correct classification with each number of leads are joined with solid red line. This line begins from 50% with no lead in the diagnostic system (dashed line). Its continuation from six leads is sketched.

system. Thus, the EEG and MEG recordings were not fully comparable in the sense of recording accuracy because the MEG recordings had about five or nine times more channels making the MEG recordings more accurate.

The patient material included 43 patients with intractable focal epilepsy. Raw EEG and MEG waveforms were reviewed independently by two experienced epileptologists, one for EEG and one for MEG.

Interictal spikes were detected in both EEG and MEG in 31, in MEG alone in 8, in EEG alone in 1, and in neither modality in 3 patients. (One patient was excluded due to poor signal quality.) Figure 17 summarizes the number of spikes and percentage of total number for all the 30 patients who had both EEG and MEG spikes. The given numbers are median values and therefore they cannot be directly summed up to get full 100%. Important in these results are that part of the spikes were possible to detect only by EEG, part of them only by MEG, and part of them with both methods indicated as electromagnetoencephalography, EMEG spikes. The difference in spike detection between EEG and MEG was not statistically significant.

Conclusions. These results are similar to our results in MCG (3, 37, 38) and confirm the two principles (1 and 2) between bioelectric and biomagnetic measurements:

EEG 70.0 65.5%
MEG 46.5 83.6% Number of spikes Percentage of total (median values)

Total EEG spikes

Total MEG spikes

Unique EEG spikes 20.0 16.4%

Common EMEG spikes 25.0 25.7%

Unique MEG spikes 20.5 34.5%

Figure 17. Similar behavior, as described above with ECG and MCG, has also been described with EEG and MEG (39). (Modified from Ref. 39.)

1. In general, both methods are equally good in detecting bioelectric sources and their diagnostic performances are about equal.
2. Because the patient groups or source details that they detect are partially overlapping, the combined use of bioelectric and biomagnetic measurements increases the diagnostic performance.

   As discussed before, the following conclusions may also be made:
3. The MEG is spatially not more accurate than the EEG.
4. The planar gradiometer MEG does not measure a vortex source and is not complementary to the EEG and therefore does not provide information essentially different from that of the EEG.
5. From the electric sources the MEG does not measure the component radial to the head. The EEG measures separately all the three orthogonal components of the electric sources.
6. Although there is no need to fix electrodes with the MEG, the dewar restricts the movement of the patient. At present there are available electrode caps that allow fixing of over 100 electrodes to the head within some 10 min.
7. The MEG needs, at least at present, a magnetically shielded room whose size due to the size of the MEG dewar exceeds normal laboratory height. This restricts the application of the MEG to certain locations. Instead, the EEG can be recorded at any location making it more easily accessible for patients.
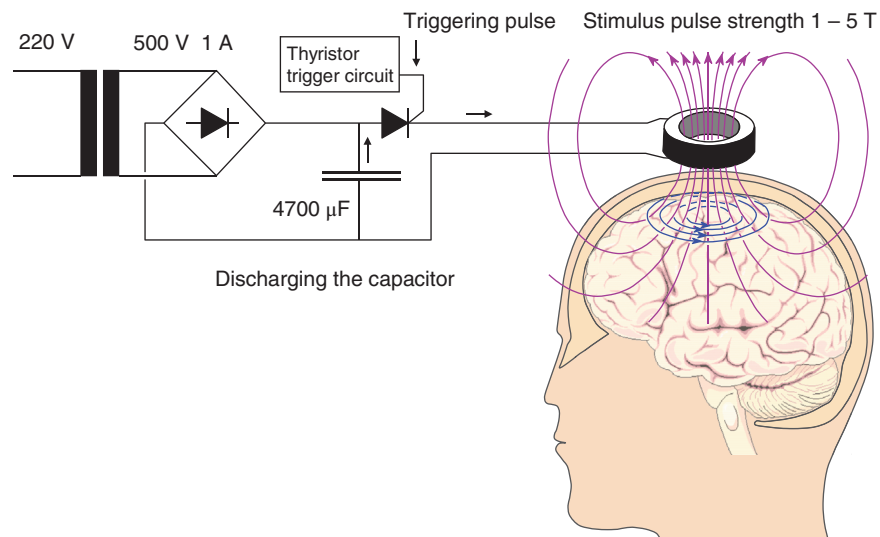
10. MAGNETIC STIMULATION

10.1. Application of the Lead Field Concept to Electric and Magnetic Stimulation

Because of reciprocity, the sensitivity distributions of electric and magnetic leads can be directly applied to electric and magnetic stimulation. In that case the sensitivity distributions of electric and magnetic measurements can be understood as stimulation energy distributions (16). This is self-evident because what is done when calculating the lead fields is actually feeding a unit current to the lead, which can be thought of as a stimulating current in the stimulation experiment.

In practice, the physical dimensions of the coils in magnetic stimulation are much larger than those used in measuring the biomagnetic fields. Therefore the results of the chapter concerning on the calculation of the lead fields of magnetic field detectors are similar, but not exactly the same as in the stimulation problems.

A magnetic stimulator includes a coil that is placed close to the surface of the skin. To induce a current into the underlying tissue, a strong and rapidly changing magnetic field must be generated by the coil. In practice, this is generated by first charging a large capacitor to a high voltage and then discharging it with a thyristor switch through a coil. The principle of a magnetic stimulator is illustrated in Figure 18 (16).

Figure 18. The principle of the magnetic stimulator.

The Faraday–Henry law states that if an electric conductor, which forms a closed circuit, is linked by a time-varying magnetic flux F, a current is observed in the circuit. This current is due to the electromotive force (emf) induced by the time-varying magnetic flux. The magnitude of emf depends on the rate of change of the magnetic flux dF/dt. The direction of emf is such that the time-varying magnetic field that results from it is always opposite to that of dF/dt; therefore,

$$\mathcal{E} = -(dF/dt) \tag{13}$$

where

E = electromotive force (emf) (V)
F = magnetic flux (Wb = Vs)
t = time (s)

Corresponding to a magnetic field $\boldsymbol{B}$, the flux $\boldsymbol{F}$, linking the circuit, is given by $\boldsymbol{F} = \int \boldsymbol{B} \cdot d\boldsymbol{S}$, where the integral is taken over any surface whose periphery is the circuit loop.

If the flux is due to a coil's own current I, the flux is defined as: $F = LI$, where L is the inductance of the coil and the emf can be written as

$$\mathcal{E} = -(dF/dt) = -L(dI/dt) \tag{14}$$

where

E = electromotive force (emf) (V)
F = magnetic flux (Wb = Vs)
L = inductance of the coil (H = Wb/A = Vs/A)
I = current in the coil (A)

The magnitude of induced emf is proportional to the rate of change of current, dI/dt. The coefficient of proportionality is the inductance L. The term dI/dt depends on the speed with which the capacitors are discharged; the latter is increased by use of a fast solid-state switch (that is fast thyristor) and minimal wiring length. Inductance L is determined by the geometry and constitutive property of the medium. The principal factors for the coil system are the shape of the coil, the number of turns on the coil, and the permeability of the core. For typical coils used in physiological magnetic stimulation, the inductance may be calculated from the following equations (41):

Multilayer Cylinder Coil. The inductance of a multilayer cylinder coil (Figure 19a) is:

$$L \approx \mu N^2 [\pi r^2/(l + 0.9r) - 0.3rs/l] \tag{15}$$
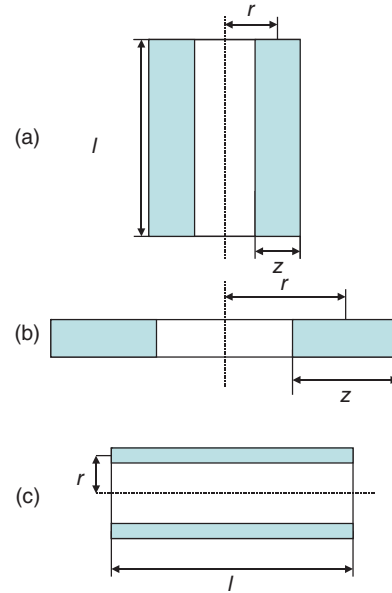
where

L = inductance of the coil (H)
μ = permeability of the coil core (Vs/Am)
N = number of turns of the coil
r = coil radius (m)
l = coil length (m)
s = coil width (m)

Figure 19. Dimensions of coils of different configuration: (a) multilayer cylinder coil; (b) flat multilayer disk coil; and (c) long single-layer cylinder coil. Expressions for the inductances of these coils are given in equations 15–17.

The following example is given on the electric parameters of a multilayer cylinder coil (41): A coil having 19 turns of $2.5\,\text{mm}^2$ copper wound in three layers has physical dimensions of $r = 18\,\text{mm}$, $l = 22\,\text{mm}$, and $s = 6\,\text{mm}$. The resistance and the inductance of the coil were measured to be $14\,\text{m}\Omega$ and $169\,\mu\text{H}$, respectively.

Flat Multilayer Disk Coil. The inductance of a flat multilayer disk coil Figure 19b is

$$L \approx \mu N^2 [\pi r^2/(0.8r + 11s)] \tag{16}$$

where N, r, and s are the same as in equation 15.

A coil having 10 turns of $2.5\,\text{mm}^2$ copper wire in one layer has physical dimensions of $r = 14$–$36\,\text{mm}$. The resistance and the inductance of the coil had the measured values of $10\,\text{m}\Omega$ and $9.67\,\mu\text{H}$, respectively.

Long Single-Layer Cylinder Coil. The inductance of a long single-layer cylinder coil (Figure 19c) is

$$L \approx \mu N^2 (\pi r^2/l) \tag{17}$$

where N, r, and l are again the same as in equation 15.

10.2. Current Distribution in Magnetic Stimulation

The magnetic permeability of biological tissue is approximately that of a vacuum. Therefore, the tissue does not have any noticeable effect on the magnetic field itself. The rapidly changing field of the magnetic impulse induces electric current in the tissue, which produces the stimulation.

Owing to the *reciprocity theorem*, the current density distribution of a magnetic stimulator is the same as the sensitivity distribution of such a magnetic detector having a similar construction. Note that in the lead field theory, the reciprocal energization equals the application of stimulating energy. The distribution of the current density in magnetic stimulation may be calculated using the method introduced in References 16 and 21 and later applied for the MEG (42).

Single Coil. The current distribution of a single coil, producing a dipolar field, was presented earlier in this article in Figure 6b. Due to technical reasons the coil used in magnetic stimulation has larger radius than the coil in magnetic field measurement. Figure 20 illustrates the distribution of the stimulation energy in the Rush-Driscoll head model when using a coil with 50 mm radius.

Quadrupolar Coil Configuration. Similarly as in the measurement of magnetic fields, also quadrupolar coils may be used in magnetic stimulation. These have the form of figure-of-eight like the planar gradiometer in the measurement systems. With a quadrupolar magnetic field the stimulating electric current field in the tissue is concentrated in a smaller region and it has a linear instead of

circular form. In some applications the result is more effective stimulation. On the other hand, a quadrupolar field decreases as a function of distance faster than that of a dipolar coil. Therefore, the dipolar coil is more effective in stimulating objects that are located deeper within the tissue.

The distribution of the stimulating electric current field of a figure of eight coil system was first calculated by Malmivuo and Puikkonen (25, 27). The first experiments with the quadrupolar magnetic field were made by Rossi et al. (41). This method has subsequently been applied to magnetic stimulation by many scientists (43, 44).

10.3. Application Areas of Magnetic Stimulation of Neural Tissue

Pioneering work in the modern magnetic stimulation has been done by Barker et al. (45) and Mills et al. (46). Magnetic stimulation can be applied to nervous stimulation either centrally or peripherally. The main benefit of magnetic stimulation is that the stimulating current density is not concentrated at the skin, as in electric stimulation, but is more equally distributed within the tissue. This is true especially in transcranial magnetic stimulation of the brain, where the high electric resistivity of the skull does not have any effect on the distribution of the
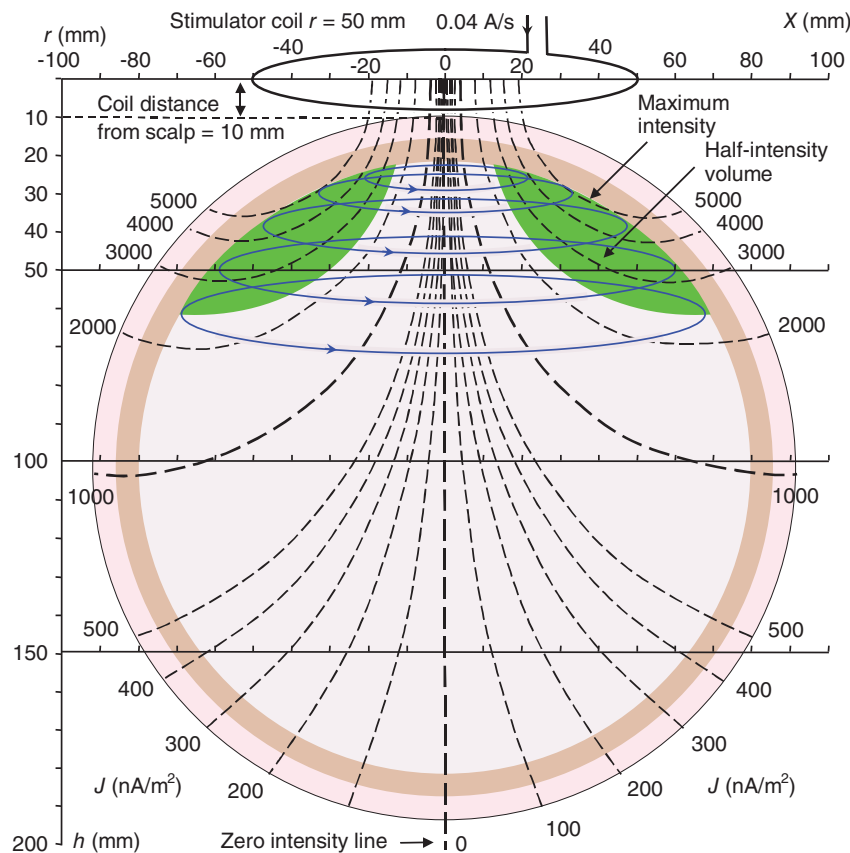
Figure 20. Calculated isointensity surfaces (dashed black lines), induced stimulation current flow lines (solid blue), and half-intensity volume (green) for a stimulation coil with 50 mm radius. The distance of the coil from the scalp is 10 mm.

stimulating current. Therefore, magnetic stimulation does not produce painful sensations at the skin, unlike stimulation of the motor cortex with electrodes on the scalp (47, 48).

Another benefit of the magnetic stimulation method is that the stimulator does not have direct skin contact. This is an advantage in the sterile operation theatre environment.

11. SUMMARY

11.1. The Source

- The origin of the biomagnetic signals is the same as that of the bioelectric signals: the bioelectric activity of the tissue.
- Theoretically, the sources of the electric and magnetic signals are the flux and vortex sources, respectively.
- The measurement sensitivity distributions of these are independent of each other.
- However, the bioelectric and biomagnetic signals are only partially independent.
- On dipolar level it has been shown that the three plus three electric and magnetic component leads are on average of similar diagnostic value and they form a "family" of six electromagnetic component leads.
- Thus, including more and more these component leads to the diagnostic system improves the diagnostic performance of the system independently whether the component leads are electric or magnetic ones.
- The amount of additional information obtained with an added component lead decreases when the number of component leads in the electromagnetic measurement system increases.
- This principle has been demonstrated earlier within the three dipolar electric component leads.
- It has not been demonstrated whether this principle is true on quadrupolar level, but there is no reason to have doubts on it.
- Combining electric and magnetic measurements improves the diagnostic performance.
- There are measurement configurations where the measurement sensitivity of a magnetic measurement greatly resembles that of an electric measurement. In such situations the information contents of the electric and magnetic signals are similar. For example:
  1. Axial magnetometer or gradiometer, where the magnetometer axis is far away from the region of heart. Its lead field in the heart region resembles one of the limb leads of the 12-lead ECG leads.
  2. Planar gradiometer whose lead field is linear in the region between the coils resembles the lead field of a bipolar EEG.

11.2. Inverse Solution

If the cardiac volume source is modeled with a magnetic dipole, the inverse solution is easy to solve by measuring the three orthogonal components of the magnetic dipole (16). Figures 4 and 5 show various methods to do this.

When recording the magnetic field with a multichannel detector, it is possible to calculate a unique solution for the inverse problem only on a surface (49, 50). This surface is usually in the cardiac problem the epicardial surface and in the brain problem the cortical surface. It is not possible to calculate a unique solution to the inverse problem for the whole three-dimensional cardiac or brain source. These inverse solutions, that is, maps of the distributions of the bioelectric sources, calculated from the magnetic field they generate, may then be used for the cardiac or brain diagnosis, respectively (23).

11.3. Special Applications

- MEG measures the brain's electric activity only in the tangential direction, while EEG measures it in all the three orthogonal directions: the two tangential directions and the one radial direction.
  - MEG is not affected by the high resistivity of the skull
  - fetal ECG is not affected by the high resistivity of the *vernix caseosa* This layer under the skin of the fetus is good electric insulator and restricts the electric recording of the fetal cardiac activity.
- Even though the skull is "transparent" to magnetic field and has high electric resistivity that blurs the electric lead field, the spatial resolutions of magnetic and electric measurements are similar in the cortical region.
- Measurement of deep sources is more difficult magnetically. With the axial magneto- or gradiometer the sensitivity is absolutely zero on the symmetry axis and thus also in the center of a spherical volume conductor. With electric measurement the sensitivity in the center of the spherical volume conductor may be arranged to be the same as anywhere else in the volume conductor. This improves the signal-to-noise ratio (51).

11.4. Technical Differences

- Magnetic measurement is contactless. Therefore, the application of multichannel magnetic measurement is fast.
- In long-term recording, especially in MEG, it is stressing for the patient to maintain static posture.
- The superconducting technology in biomagnetic recordings gives the possibility to extend the frequency range down to DC, that is, to 0 Hz.
- Due to the very low level of magnetic signal amplitude, especially the MEG instrumentation is much more expensive than the electric one.

11.5. Magnetic Stimulation

- The distribution of the stimulation current in magnetic stimulation is calculated with the same

equations as the measurement sensitivity distribution in magnetic measurements.

- Due to the larger coils in magnetic stimulation the focusing of the stimulation energy is not as good as the focusing of the measurement sensitivity.
- Because the skull is "transparent" to magnetic field, the stimulation current density in the scalp is of the same order as in the cortical brain region. Therefore, unlike in electric stimulation, the magnetic stimulation causes no pain, not even any sensation to the patient.

12. CONCLUSIONS

The bioelectric and biomagnetic measurements measure the same physiological phenomenon: the bioelectric activity of the tissue. Their signal processing and interpreting methods are similar. The biomagnetic measurement technology is more expensive than the bioelectric one. Especially this holds on MEG due to its very low signal amplitude.

The bioelectric and biomagnetic measurements give partially independent information of the source, and therefore they complement each other. It is important to understand what is the amount and content of the additional diagnostic information of biomagnetic measurements to justify their higher price. Therefore, the biomagnetic measurements must have verified benefits over the bioelectric ones to be worth to apply. Biomagnetic measurements have some special properties that cannot be realized with bioelectric measurements. If such measurements give vital diagnostic information, it strongly justifies the use of biomagnetic measurements.

Magnetic stimulation of the brain, unlike the electric stimulation, does not cause any sensation to the patient that is a great benefit. Due to the large coil dimension, it does not have equally good spatial resolution as the electric stimulation.

BIBLIOGRAPHY*

1. H. C. Örsted. *J. Chem. Phys.* **1820**, *29*, pp 275–281.
2. J. C. Maxwell. *Phil. Trans. R. Soc. (Lond.).* **1865**, *155*, pp 459–512.
3. J. Malmivuo. *Brain Topogr.* **2012**, *25*, pp 1–19.
4. J. Malmivuo, J. Honkonen, and K. Wendel. Did Jan Swammerdam Do the First Electric Stimulation Over 100 Years Before Luigi Galvani? in Roa Romero L. M., Ed., *XIII Mediterranean Conference on Medical and Biological Engineering and Computing Seville*, September 25–28, 2013; IFMBE Proceedings 41, pp 13–16.
5. L. Galvani. *De Bononiesi Scientarium et Ertium Instituto atque Academia Commentarii.* **1791**, 7, pp 363–418.

6. C. Matteucci. *Ann. Chim. Phys. (2ème série).* **1838**, *68*, pp 93–106.
7. L. Nobili. *J. Chem. Phys.* **1825**, *45*, pp 249–254.
8. G. M. Baule and R. McFee. *Am. Heart J.* **1963**, *55* (7), pp 95–96.
9. J. A. d'Arsonval. *Arch. Physiol. Norm. Pathol. (1ère série).* **1893**, *5*, pp 401–408.
10. R. Plonsey. *Bioelectric Phenomena*. McGraw-Hill: New York, 1969; p 380.
11. D. B. Geselowitz. *Biophys. J.* **1967**, *7* (1), pp 1–11.
12. J. A. Stratton. *Electromagnetic Theory*. McGraw-Hill: New York, 1941.
13. W. R. Smythe. *Static and Dynamic Electricity*, 3rd ed.; McGraw-Hill: New York, 1968; p 623.
14. J. D. Jackson. *Classical Electrodynamics*, 2nd ed.; John Wiley & Sons: New York, 1975; p 641.
15. D. B. Geselowitz. *IEEE Trans. Magn.* **1970**, *6* (2), pp 346–347.
16. J. Malmivuo and R. Plonsey. *Bioelectromagnetism: Principles and Applications of Bioelectric and Biomagnetic Fields*. Oxford University Press: New York, 1995; p 480.
17. H. L. F. Helmholtz. *Ann. Phys. Chem.* **1853**, *89*, pp 211–233, 354–377.
18. J. A. Malmivuo, J. O. Lekkala, P. Kontro, L. Suomaa, and H. Vihinen. *J. Phys. E. Sci. Instrum.* **1987**, *20* (1), pp 151–164.
19. K.-P. Estola and J. A. Malmivuo. *J. Phys. E. Sci. Instrum.* **1982**, *15*, pp 1110–1113.
20. D. Robbes. *Sens. Actuators.* **2006**, *A 129*, pp 86–93.
21. J. A. Malmivuo. *Acta Polytechnol. Scand.* **1976**, *39*, p, 112
22. W. H. Barry, W. M. Fairbank, D. C. Harrison, K. H. Lehrman, J. A. V. Malmivuo, and J. P. Wikswo, Jr. *Science*. **1977**, *198* (12), pp 1159–1162.
23. E.-S. Shin, Y.-Y. Lam, A.-Y. Her, J. Brachmann, F. Jung, and J.-W. Park. *Int. J. Cardiol.* **2017**, *228*, pp 948–952.
24. J. Malmivuo, V. Suihko, and H. Eskola. *IEEE Trans. Biomed. Eng.* **1997**, *44* (3), pp 196–208.
25. J. Malmivuo and J. Puikkonen. Sensitivity Distribution of Multichannel MEG-Detectors, in *Abstract Book of the 6th International Conference on Biomagnetism;* Tokyo, Japan, August 27–30, 1987; pp 112–113.
26. S. Rush and D. A. Driscoll. *IEEE Trans. Biomed. Eng.* **1969**, *16*, pp 15–22.
27. J. Malmivuo and J. Puikkonen. *Tampere Univ. Technol. Inst. Biomed. Eng. Rep.* **1988**, *1* (7), p 35.
28. J. Malmivuo and V. Suihko. *IEEE Trans. Biomed. Eng.* **2004**, *51* (7), pp 1276–1280.
29. T. F. Oostendorp, J. Delbeke, and D. F. Stegeman. *IEEE Trans. Biomed. Eng.* **2000**, *47* (11), pp 1487–1492.
30. R. Hoekema, G. J. M. Huiskamp, G. H. Wieneke, F. S. S. Leijten, C. W. M. van Veelen, P. C. van Rijen, and A. C. van Huffelen. *Biomed. Technik.* **2001**, *46B* pp 103–105.
31. R. Plonsey. *IEEE Trans. Biomed. Eng.* **1972**, *19* (3), pp 239–244.
32. S. Rush. *IEEE Trans. Biomed. Eng.* **1975**, *22* (3), pp 157–167.
33. P. M. Morse and H. Feshbach. *Methods of Theoretical Physics, Part I*. McGraw-Hill: New York, 1953; p 997.
34. R. Plonsey and R. Collin. *Principles and Applications of Electromagnetic Fields*. McGraw-Hill: New York, 1961; p 554.
35. J. Malmivuo, J. Nousiainen, O. S. Oja, and A. Uusitalo. General Solution for the Application of Magnetocardiography, in *Proc. of the World Congress on Medical Physics and Biomedical Engineering; Chicago, USA, July 23–28*, 2000, p MO-B205-1.

* The references (or links to them) may be found from: www.bem.fi > library.

36. J. Malmivuo, J. Nousiainen, O. S. Oja, and A. Uusitalo. General Solution for the Application of Magnetocardiography, in Nowak H.; Haueisen J.; Giessler F.; Huonker R., Eds., *Proc. of the BIOMAG 2002, 13th International Conference on Biomagnetism; Jena, Germany*, August 10–14, 2002, pp. 546–549.

37. J. Malmivuo. The Solution for the Independence of Bioelectric and Biomagnetic Signals is Confirmed, in *Proceedings of the 35th Annual International Conference of the IEEE Engineering in Medicine and Biology Society; Osaka, Japan*, July 3–7, 2013.

38. O. S. Oja. *Vector Magnetocardiogram in Myocardial Disorders*. MD thesis, University of Tampere, Medical Faculty, 1993, p 168.

39. P. A. Lachenbruch and M. R. Mickey. *Technometrics*. **1968**, *10*, pp 1–11.

40. M. Iwasaki, E. Pestana, R. C. Burgess, H. O. Lüders, H. Shamoto, and N. Nakasato. *Epilepsia*. **2005**, *46* (1), pp 59–68.

41. R. Rossi, J. Puikkonen, J. A. Malmivuo, H. J. Eskola, and V. Häkkinen. *Tampere Univ. Technol. Inst. Biomed. Eng. Rep.* **1987**, *1* (6), p 25.

42. J. A. Malmivuo. *Med. Biol. Eng. Comput.* **1980**, *18* (3), pp 365–70.

43. S. Ueno, T. Tashiro, and K. Harada. *J. Appl. Phys.* **1988**, *64*, pp 5862–5864.

44. R. J. Ilmoniemi, J. Virtanen, J. Ruohonen, J. Karhu, H. J. Aronen, R. Näätänen, and T. Katila. *Neuroreport*. **1997**, *8* (16), pp 3537–3540.

45. A. T. Barker, R. Jalinous, and I. L. Freeston. *Lancet*. **1985**, *1* (8437), pp 1106–1107.

46. K. R. Mills, N. M. F. Murray, and C. W. Hess. *Neurosurgery*. **1987**, *20*, pp 164–168.

47. I. Rimpiläinen, H. J. Eskola, V. Häkkinen, and P. Karma. *Electromyogr. Clin. Neurophysiol.* **1991**, *31*, pp 259–263.

48. I. Rimpiläinen. *Magnetic Stimulation of Facial Nerves*. MD thesis, University of Tampere, Medical Faculty, 1994, p 112.

49. Y. Yamashita. *IEEE TBME*. **1982**, *29* (11), pp 719–725.

50. Y. Yamashita and E. Takahashi. *IEEE TBME*. **1984**, *31* (9), pp 611–621.

51. O. Väisänen and J. Malmivuo. *J. Physiol. Paris*. **2009**, *103* (6), pp 306–314.

JAAKKO MALMIVUO

Technische Universität Berlin, Berlin, Germany